ALGERIAN DEMOCRATIC AND POPULAR REPUBLIC

MINISTRY OF HIGH EDUCATATION AND

SCIENTIFIC RESEARCH

Echahid Cheikh Larbi Tebessi University- Tebessa

Faculty of Exact Sciences and Natural and Life Sciences

Department: Material Sciences

Master Thesis

Domain: Material Sciences

SPECIALTY

Materials Physics

THEME

Effect of Al doping and TiO_2 interlayer on the physical properties of ZnO thin films deposited by spray pyrolysis

By:

OUAHAB Dhoha

Jury committee:

President:	**BENKHEDIR Mohammed Lotfi**	**Prof.**	**Echahid Cheikh Larbi Tebessi University- Tebessa**
Advisor:	**HANINI Faouzi**	**M.C.A.**	**Echahid Cheikh Larbi Tebessi University- Tebessa**
Examiner:	**FERDI Abdelhamid**	**M.C.A.**	**Echahid Cheikh Larbi Tebessi University- Tebessa**

Defended on: 10/06/2025

Note :.....18,50..... Mention :.....Très.....

الجمهورية الجزائرية الديمقراطية الشعبية
PEOPLE'S DEMOCRATIC REPUBLIC OF ALGERIA
وزارة التعليم العالي و البحث العلمي
MINISTRY OF HIGHER EDUCATION AND SCIENTIFIC RESEARCH
جامعة الشهيد الشيخ العربي التبسي
ECHAHID CHEIKH LARBI TEBESSI UNIVERSITY, TEBESSA
كلية العلوم الدقيقة وعلوم الطبيعة والحياة
FACULTY OF EXACT SCIENCES, NATURAL AND LIFE SCIENCES

Déclaration sur l'honneur de non-plagiat

(A joindre obligatoirement au mémoire, remplie et signée).

Je soussigné (e) :

Nom, Prénom : OUAHAB Dhoha.

Régulièrement inscrit(e):en master au département : Sciences de la matière

N° de carte d'étudiant : 202034020021

Année universitaire : 2024/2025

Domaine : Sciences de la matière

Filière : physique

Spécialité : Physique des matériaux

Intitulé du mémoire :

Effect of Al doping and TiO_2 interlayer on the physical properties of ZnO thin films deposited by spray pyrolysis.

Atteste que mon mémoire est un travail original et que toutes les source utilisées ont été indiquées dans leur totalité je certifie également que je n'ai ni recopié ni utilisé des idées ou des formulations tirées d'un ouvrage article ou mémoire en version imprimée ou électronique sans mentionner précisément leur origine et que les citation intégrales sont signalées entre guillemets

Sanctions en cas de plagiat prouvé

L'étudiant sera convoqué de vent le conseil de discipline les sanctions prévues selon la gravité de plagiat sont :

- L'annulation de mémoire avec possibilité de la refaire sur un sujet diffèrent
- L'exclusion d'une année du master
- L'exclusion définitive

Fait à Tébessa, le 29/06/2025

Signature de l'étudiant (e) :

الجمهورية الجزائرية الديمقراطية الشعبية
PEOPLE'S DEMOCRATIC REPUBLIC OF ALGERIA
وزارة التعليم العالي و البحث العلمي
MINISTRY OF HIGHER EDUCATION AND SCIENTIFIC RESEARCH
جامعة الشهيد الشيخ العربي التبسي
ECHAHID CHEIKH LARBI TEBESSI UNIVERSITY, TEBESSA
كلية العلوم الدقيقة وعلوم الطبيعة والحياة
FACULTY OF EXACT SCIENCES, NATURAL AND LIFE SCIENCES

Département : Sciences de la matière.

Filière : …Physique……

Spécialité :…… Physique Des Matériaux……

Année universitaire 2024/2025

Formulaire de levée de réserves après soutenance d'un Mémoire de Master

Données d'identification du candidats(es) :

Nom et prénom du candidat : …… **Dhoha Ouahab** ……

Intitulé du Sujet: **Effect of Al doping and TiO_2 interlayer on the physical properties of ZnO thin films deposited by spray pyrolysis.**

Données d'identification du membre de jury :

Nom et prénom : …… Benkhedir Mohammed Loutfi ……

Grade :……**Professeur**……

Lieu d'exercice : Université Echahid Cheihk Larbi Tebessi- Tébessa

Vu le procès-verbal de soutenance de la thèse sus citée comportant les réserves suivantes :

……

……

……

……

……

……

Et après constatation des modifications et corrections suivantes :

……

……

……

……

……

……

Je déclare en ma qualité de président de jury de soutenance que le mémoire cité remplit toutes les conditions exigées et permet au candidat de déposer son mémoire en vue de l'obtention de l'attestation de succès.

Le 29/06/2025

Président de jury de soutenance :

Pr. Mohammed Loutfi Benkhedir

ALGERIAN DEMOCRATIC AND POPULAR REPUBLIC

MINISTRY OF HIGH EDUCATATION AND

SCIENTIFIC RESEARCH

Echahid Cheikh Larbi Tebessi University- Tebessa

Faculty of Exact Sciences and Natural and Life Sciences

Department: Material Sciences

Master Thesis

Domain: Material Sciences

SPECIALTY

Materials Physics

THEME

Effect of Al doping and TiO_2 interlayer on the physical properties of ZnO thin films deposited by spray pyrolysis

By:

OUAHAB Dhoha

Jury committee:

President:	**BENKHEDIR Mohammed Lotfi**	**Prof.**	**Echahid Cheikh Larbi Tebessi University- Tebessa**
Advisor:	**HANINI Faouzi**	**M.C.A.**	**Echahid Cheikh Larbi Tebessi University- Tebessa**
Examiner:	**FERDI Abdelhamid**	**M.C.A.**	**Echahid Cheikh Larbi Tebessi University- Tebessa**

Defended on: 10/06/2025

Note :……. Mention :……..……



«يَرْفَعِ اللَّهُ الَّذِينَ آمَنُوا مِنكُمْ وَالَّذِينَ أُوتُوا الْعِلْمَ دَرَجَاتٍ»

المجادلة – الآية 11

ملخص

في هذه الدراسة، تمت دراسة تأثير تطعيم الألمنيوم وطبقة ثنائي أكسيد التيتانيوم (TiO_2) الوسيطة على الخصائص التركيبية والبصرية لأفلام أكسيد الزنك (ZnO) الرقيقة. تم ترسيب أفلام غير مُطعمة (ZG) وأفلام مُطعمة بالألمنيوم (AZG) على ركائز زجاجية، مع وبدون طبقة TiO_2 الوسيطة، باستخدام تقنية التحلل الحراري بالرش. خضعت العينات لتحاليل باستخدام مطيافية الأشعة تحت الحمراء ذات تحويل فورييه (FTIR) ومطيافية الأشعة فوق البنفسجية–المرئية (UV–Vis). التحليل باستخدام مطيافية الأشعة تحت الحمراء أكد بشكل خاص وجود أنماط اهتزازية مرتبطة بـ TiO_2 وZnO ، بالإضافة إلى الدمج الناجح للألمنيوم (Al) داخل بلورة ZnO .أظهرت نتائج UV–Vis تأثيرات كبيرة على الشفافية وطاقة أورباخ، حيث أدى التطعيم بالألمنيوم وحده إلى تقليل فجوة النطاق. تم تحديد معامل الانكسار للأفلام الرقيقة عن طريق استخدام أطياف النفاذية UV–Vis.

الكلمات المفتاحية: التحلل الحراري بالرش؛ أفلام أكسيد الزنك المطعمة بالألمنيوم؛ طبقة TiO_2 الوسيطة؛ مطيافية الأشعة تحت الحمراء ذات تحويل فورييه (FTIR) ؛ الخصائص البصرية.

.

Abstract

In this study, the effects of Aluminum doping and a titanium dioxide (TiO_2) interlayer on the structural and optical properties of ZnO thin films were investigated. Undoped (ZG) and Al-doped ZnO (AZG) films were fabricated on glass substrates, with and without a TiO_2 interlayer, using spray pyrolysis technique. The samples underwent characterization via FTIR, and UV–Vis spectroscopy. FTIR analysis particularly confirmed the presence of vibrational modes related to TiO_2 and ZnO as well as the successful incorporation of Al into the ZnO crystal. UV–Vis results indicated significant impacts on transparency and the Urbach energy, with Al doping alone reducing the band gap. The determination of the refractive index of the thin films has been performed by exploitation UV-Vis transmittance spectra.

Keywords: Spray pyrolysis; Al doped ZnO films; TiO_2 interlayer; FTIR; Optical properties.

.

Résumé

Dans cette étude, les effets du dopage à l'aluminium et d'une couche intermédiaire de dioxyde de titane (TiO_2) sur les propriétés structurales et optiques des couches minces de ZnO ont été étudiés. Des couches de ZnO non dopées (ZG) et dopées à l'aluminium (AZG) ont été élaborées sur des substrats de verre, avec et sans couche intermédiaire de TiO_2, en utilisant la technique de spray pyrolyse. Les échantillons ont été caractérisés par spectroscopie FTIR et UV-Vis. L'analyse FTIR a particulièrement confirmé la présence de modes vibrationnels liés au TiO_2 et au ZnO, ainsi que l'incorporation réussie de l'aluminium dans le cristal de ZnO. Les résultats UV-Vis ont indiqué des impacts significatifs sur la transparence et l'énergie d'Urbach, le dopage à l'aluminium seul réduisant la bande interdite. La détermination de l'indice de réfraction des couches minces a été réalisée en exploitant les spectres de transmission UV-Vis.

Mots-clés : Spray pyrolyse ; Films ZnO dopé Al; Couche intermédiaire de TiO_2 ; FTIR ; propriétés optiques.

Acknowledgements

*Above all, we are thankful to "**ALLAH**", the Almighty, for providing us with the endurance, courage, and faith necessary to finish this work. Then, we ask Allah to support our scientific pursuits and provide us the information we need to help others and progress humanity.*

This work was carried out at the Echahid Cheikh Larbi University Tébessi-Tébessa's Applied and Theoretical Physics Laboratory.

*I would like to express my gratitude to **Dr. HANINI Faouzi** lecturer 'A' at the Department of Material Sciences, Faculty of Exact Sciences and Natural and Life Sciences, Echahid Cheikh Larbi University Tébessi-Tébessa, for letting us work under his supervision as our academic supervisor and for his wise counsel and suggestions, all of which were very beneficial to us as we conducted research for our master's thesis.*

*I also want to express our gratitude to the evaluation committee members **Pr. BENKHEDIR Mohammed Lotfi** and **Dr. FERDI Abdelhamid** who honoured us by agreeing to review and improve this work.*

Finally, but just as importantly, we want to express our gratitude to our loving parents, relatives, and friends for their encouragement and support.

DEDICATION

To my parents (Ali /Halima),

To my self,

To my brothers (Fares / Koussay),

To my sisters (Amani / Maroua / Souraya / Belkis/ Wissem).

Dhoha .

TABLE OF CONTENTS

TABLE OF CONTENTS

ملخص	I
Abstract	II
Résumé	III
Acknowledgements	IV
Dedication	V
Table of contents	VI
List of tables	IX
List of figures	X
List of symbols	XII
Introduction	1
Chapter I. Bibliographic studies of ZnO and TiO_2 thin films	
I.1. Transparent Conductive Oxides	3
I.1.1. TCO Materials	3
I.1.2. Applications of TCO	4
II.1. Metal Oxides	5
II.1.1. Classification of metal oxides	5
II.1.2. Doping of metal oxides	6
III.1. Zinc oxide (ZnO)	7
III.1.1. Properties of ZnO	7
A. Structural properties of ZnO	7
B. Optical properties of ZnO	9
C. Electrical properties of ZnO	10
III.1.2. The dopants of ZnO	11
III.1.3. Applications of ZnO thin films	12
III.2. Titanium dioxide (TiO_2)	13
III.2.1. Properties of TiO_2	13
A. Structural properties of TiO_2	13
B. Optical properties of TiO_2	14
C. Electrical properties of TiO_2	14
IV.1 Overview on thin film	15

IV.1.1. General concept of thin films 15
IV.1.2. Principal of thin films deposition 15
IV.1.3. Classification of thin film deposition techniques 16
IV.1.3.1. Physical deposition techniques 16
1. In vacuum 16
i. Evaporation techniques 16
a. Vacuum thermal evaporation technique 17
b. Electron beam evaporation 18
ii. Pulsed-laser deposition 18
2. In plasma 19
a) Sputtering technique 19
IV.1.3.2. Chemical deposition techniques 20
1) In solution 20
a. Sol-gel technique 20
b. Spray Pyrolysis technique 21
Chapter II. Elaboration technique and characterization tools
Part One: elaboration of thin films 23
II.1 Preparation of the substrate 23
II.1.1. Choice of substrates 23
II.1.2. Cleaning the substrates 23
II.2 The choice of spray pyrolysis technique 24
II.3. Preparation of solution 24
1.For doped and undoped ZnO 24
2. For Titanium dioxide (TiO_2) 25
Part two: Characterization techniques of thin films 27
II.1. Structural characterization and measurement 27
II.1.1. Fourier Transform Infrared Spectroscopy (FTIR) 27
II.2. Optical characterization and measurement 28
II.2.1. Ultraviolet-visible spectroscopy 28

II.2.1.1. Determination of film thickness (d) and refractive index (n) 30
II.2.1.2. Determination of absorption coefficient (α) 31
II.2.1.3. Determination of optical band gap (E_g) 31
II.2.1.4. Determination of Urbach energy (E_u/E_{00}) 32
Chapter III. Results and discussion
III.1. Structural Studies 34
III.1.1. FTIR Analysis 34
III.2. Optical properties 39
III.2.1. UV–vis analysis 39
III.2.1.1. Calculation of the Refractive Index 40
III.2.1.2. Band gap and Urbach energy 41
a) Band gap 41
b) Urbach energy 44

LIST OF TABLES

Table.I.1	TCO materials	**04**
Table.I.2	Example of some metal oxides	**05**
Table.I.3	Some properties of ZnO in the wurtzite structure	**08**
Table.I.4	Some electrical properties of ZnO	**11**
Table.I.5	The dopants of ZnO	**12**
Table.I.6	Crystal structure data of TiO_2	**14**
Table II.1	Different products used for the preparation of our thin films.	**24**
Table II.2	The experimental conditions for the spray deposition of thin films	**25**
Table III.1	Comparative Analysis of vibrational modes of ZG thin film	**34**
Table III.2	Comparative Analysis of vibrational modes of AZG thin film	**35**
Table III.3	Comparative Analysis of vibrational modes of TG thin film	**37**
Table III.4	Comparative Analysis of vibrational modes of ZTG thin film	**38**
Table III.5	Comparative Analysis of vibrational modes of AZTG thin film	**39**
Table III.6	Presents the refractive indices for the ZG, AZG, TG, ZTG and AZTG samples determined by UV-Visible transmission measurements	**40**
Table III.7	Tauc plot for the optical band gap estimation of ZG, AZG, TG, ZTG, and AZTG thin films	**43**
Table III.8	Estimated Urbach energy of ZG, AZG, TG, ZTG, and AZTG thin films	**45**

LIST OF FIGURES

Figure.I.1	Some applications of TCOs	**04**
Figure.I.2	Representation of the energy level of the doping element (n-type)	**06**
Figure.I.3	Representation of the energy level of the doping element (p-type)	**06**
Figure.I.4	a) Zinc oxide Powder and b) Photograph of a natural crystal of Zincite	**07**
Figure.I.5	Crystal structures of ZnO: a) rocksalt, b) zinc blend c) wurtzite	**08**
Figure.I.6	(a) Wurtzite structure of ZnO and (b) Wurtzite unit cell of ZnO	**09**
Figure I.7	ZnO band structure	**11**
Figure I.8	Planar Ti_3O building-block representation (left) and TiO_6 polyhedra (right) for the TiO_2 phases rutile (a), anatase (b) and brookite (c) (Ti (white); O (red))	**13**
Figure I.9	TiO_2 band structure for rutile (a), anatase (b) and brookite (c)	**15**
Figure I.11	Classification of thin film deposition technique	**16**
Figure I.12	Schematic of Vacuum thermal evaporation technique	**17**
Figure I.13	Schematic diagram of electron beam evaporation	**18**
Figure I.14	General diagram of PLD	**19**
Figure I.15	Sputtering system diagram	**20**
Figure I.16	Sol-gel process diagram (a): Spin-coating, (b): Dip-coating	**21**
Figure I.17	Shows the spray pyrolysis technique	**22**
Figure II.1	Glasses substrates	**23**
Figure II.2	The experimental setup used	**25**
Figure II.3	Schematically represents the preparation steps of thin films using the spray pyrolysis technique	**26**
Figure II.4	Experimental device for FT-IR spectroscopy (JASCO - 4X)	**28**

Figure II.5	Schematic spectrometer of UV-Vis	**29**
Figure II.6	Experimental device for UV-Vis-NIR spectroscopy (JASCO V-730)	**29**
Figure II.7	Determination of interference fringes for find the refractive index and film thickness	**30**
Figure II.8	Determination of optical band gap	**32**
Figure II.9	Example of the determination of Urbach energy	**33**
FigureIII.1	FTIR spectrum of ZG thin film	**34**
Figure III.2	FTIR spectrum of AZG thin film	**35**
Figure III.3	FTIR spectrum of TG thin film	**36**
Figure III.4	FTIR spectrum of ZTG thin film	**37**
Figure III.5	FTIR spectrum of AZTG thin film	**38**
Figure III.6	Optical transmission spectra of ZG, AZG, TG, ZTG, and AZTG thin films	**39**
Figure III.7	Direct band gap energy (Tauc's plot) determination of ZG and AZG	**41**
Figure III.8	Direct band gap energy (Tauc's plot) determination of ZG and AZG	**42**
Figure III.9	Direct band gap energy (Tauc's plot) determination of ZTG and AZTG	**42**
Figure III.10	Plots of Lnα as a function of photon energy for Urbach energy estimation of ZG, AZG, TG, ZTG, and AZTG thin films	**44**

List of symbols

Symbol	Signification	Unit
T	Optical transmittance	%
d	Film thickness	nm
ρ	The electrical resistivity	Ω.cm
μ_n	Mobility of electrons	$m^2.V^{-1}.s^{-1}$
σ	Electrical conductivity	$\Omega^{-1}.cm^{-1}$
α	Absorption coefficient	cm^{-1}
m	Mass	g
M	Mass molar	g/mol
C	Solution concentration	mol/ l
V	Volume	l
I	Intensity of light	
I_0	Initial light intensity	
E_g	Energy of optical band gap	eV
E_u/E_{00}	Urbach energy	eV
k	Extinction coefficient	
n	Refractiveindex	
S	Refractive index of the substrate	
λ	Wavelength of incident photon	nm
$h\nu$	Energy of incident photon	eV

Introduction

Spray pyrolysis process is well known for its capacity to provide ZnO thin films with excellent characteristics and suitable for various applications [1]. It also has several benefits, including low cost and simple control over chemical purity and homogeneity. It has recently been demonstrated that using the double-layer structure is a successful method of enhancing the characteristics of metal oxides. There have been numerous attempts to alter ZnO thin-films optical, chemical, and physical characteristics by mixing them with other oxides such as TiO_2, SnO_2 [2] and SiO_2 [3].

In this work, we present the preliminary results about the preparation of spray pyrolysis Al doped ZnO thin films prepared on glass substrates with and without TiO_2 inter - layer and particularly the study of their optical properties.

The investigated thin films of pure and Al-doped ZnO deposited via spray pyrolysis. Zinc Acetate Dehydrate Zn $[OOCCH_3]_2.2H_2O$ (99 %) with a concentration of 0.2 M was used as the precursor, Aluminum sulfate octadecahydrate $Al_2(SO_4)_3 \cdot 18H_2O$ (99 %) as the dopant, and Ethanol (97%) as the solvent. The procedure of the preparation of TiO_2 solution includes the dissolution of titanium isopropoxide with a concentration of 0.2 M in isopropanol alcohol (98%).

Introducing TiO_2 as an interlayer for Al–ZnO/glass can further influence the properties of ZnO films. TiO_2 is recognized for its excellent transparency, wide band gap, and good optical properties. Accordingly, including TiO_2 enhances the optical properties of ZnO films and optimizes their optoelectronic characteristics, making them ideal for device applications requiring both high transparency and conductivity.

This scientific study examines both the TiO_2 interlayer and Al doping affect the physical characteristics of ZnO thin films using ***FTIR*** and ***UV-Vis*** spectra analysis.

This work is organized into three separate chapters, in addition to an introduction and a conclusion.

- **In Chapter I**, a brief overview of thin films is provided, followed by a particular focus on the Spray pyrolysis process used for the elaboration of our thin films. Furthermore, in this regard, a bibliographic study is presented

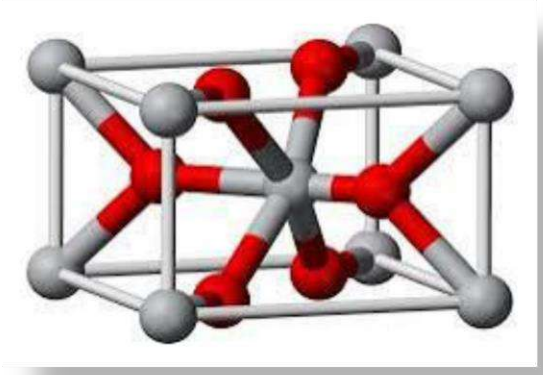
concerning the various properties of ZnO and TiO_2, as well as their areas of application,

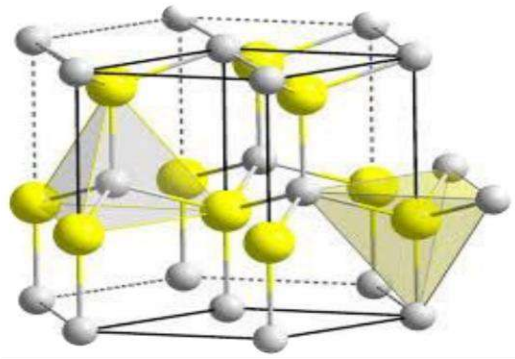
- **Chapter II** presents a comprehensive overview of the different stages involved in the elaboration of our thin films using the spray pyrolysis technique, along with various methods and different characterization techniques,

- Finally, in the **last chapter**, the experimental results related to the samples prepared by the spray pyrolysis method are presented along with their interpretations.

Chapter I

Bibliographic studies of ZnO and TiO_2 thin films







I.1. Transparent Conductive Oxides

A metal oxide in the thin film form is transparent to visible light and conducts electricity, so it is called a transparent conductive oxide (TCO). The TCOs used in technological applications should have the following characteristics: First, they should be transparent for the visible part of light with transmittance > 80 %. Second, they should be a good conductor of electricity with a high enough concentration of electrical carriers, i.e. an electron or hole concentration $\geq 10^{19}$ cm^{-3} and with a sufficiently large mobility ≥ 1 cm^2 $V^{-1}s^{-1}$ [4].

Transparent conductive oxides (TCO) can be classified as either n-type or p-type semiconductors, depending on the predominant type of charge carriers. Nevertheless, practical applications remain largely confined to n-type TCOs, as they are the only ones that currently exhibit an optimal balance between high electrical conductivity and optical transparency [5].

The majority of research on developing highly transparent and conductive thin films has concentrated on (n)-type semiconductors made from metal oxides that ideally have a wide band gap (>3eV). Indium tin oxide (ITO) has long been the most commonly used material for a wide range of applications, including solar cells and flat screens. However, the high cost and limited availability of indium have driven researchers to search for alternative materials. Zinc oxide (ZnO), both doped and undoped, has emerged as a promising candidate due to its superior transparency in the visible spectrum, low resistivity comparable to ITO thin films, affordability, abundance, and non-toxic nature [6,7].

I.1.1. TCO Materials

Numerous material systems have been extensively investigated as potential candidates for transparent conducting oxides (TCOs). Table I.1 summarizes commonly used TCO host materials along with their corresponding dopants, covering binary, ternary, and multicomponent oxide systems [8].

Table I.1. TCO materials [8].

Material	Dopant or compound
In_2O_3	Sn,Ge,Mo,F,Ti,Zr,Hf,Nb,Ta,W,Te
SnO_2	Sb,F,As,Nb,Ta
ZnO	Al,Ga,B,In,Y,Sc,F,V,Si,Ge,Ti,Zr,Hf
CdO	In, Sn
ZnO- SnO_2	Zn_2SnO_4, $ZnSnO_3$
ZnO-In_2O_3	$Zn_2In_2O_5$, $Zn_3In_2O_3$
In_2O_3- SnO_2	$In_4Sn_3O_{12}$
CdO- SnO_2	Cd_2SnO_4, $CdSnO_3$
CdO- In_2O_3	$CdIn_2O_4$
ZnO- In_2O_3- SnO_2	$Zn_2In_2O_5$-$In_4Sn_3O_{12}$
CdO- In_2O_3- SnO_2	$CdIn_2O_4$-Cd_2SnO_4

I.1.2. Applications of TCO

TCOs are materials that combine high transparency in the visible spectrum with excellent electrical conductivity, enabling the coexistence of optical and electrical properties. These unique characteristics have garnered significant attention in research and industry, making TCOs essential for numerous applications and components**:** Solar cell, Optoelectronic systems, Gas sensors, Touch screens, Flat screens, Electrochromic mirrors and windows, Windows reflecting heat (Figure.I.1) [7].

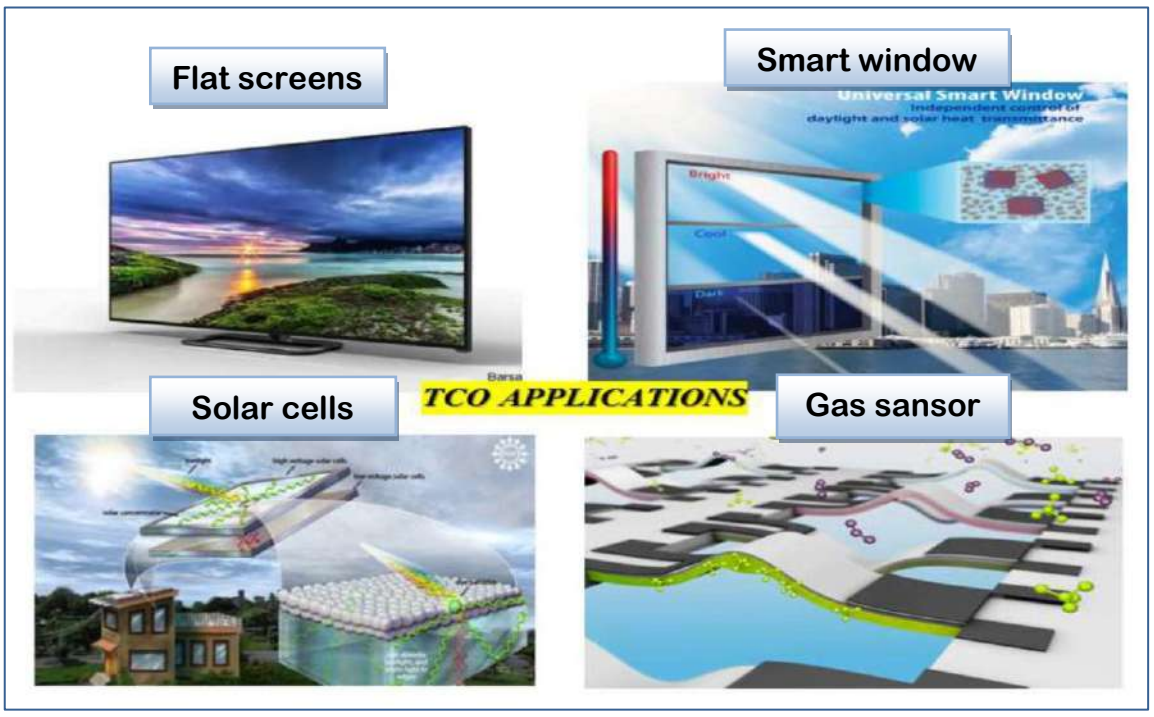


Figure I.1. Some applications of TCOs [9].

II.1. Metal Oxides

Metal oxides (MO) are homogeneous solid phases containing one or more types of metal cations of different oxidation states ($M1_xM2_yO_z$), where M is the chemical symbol of the Metal atom considered, O the symbol of the oxygen atom, "x" and "y" and "z" natural integers, among the important metal oxide Al_2O_3, ZnO, Cr_2O_3, CuO, Fe_2O_3, SnO_2, and $BaTiO_3$. The cations combine with the O^{-2} (oxide ions) to give well-defined crystallographic structures. Generally, to obtain the metal oxide, the oxygen is added to a metallic element (oxidation reaction). The methods of preparation, the chemical nature of the cations as well as the chemical composition of these oxides are of fundamental importance. These cations lead to the variation of physical properties such as optical transmittance, electrical conductivity and specific surface area, thus inducing significant changes in the electrochemical and catalytic behavior of these materials. The oxide group is therefore one of the most varied classes of minerals in physical and chemical properties [10].

II.1.1. Classification of metal oxides

There are two principal categories by which metal oxides can be classified (Table I.2) [11]:

(i) The first type is n-type oxides (electron conduction oxides). These oxides are widely applied in gas sensors owing to their excellent stability and attractive chemisorption properties,

(ii) The second group has p-type oxides (hole-conducting oxides). These oxides are quite reactive since they tend to quickly react with air and exchange oxygen. However, p-type oxides are employed in certain applications, for example, high-temperature oxygen sensors.

Table I.2. Example of some metal oxides [11].

n-type metal oxide	p-type metal oxide
TiO_2	CuO
ZnO	NiO
SnO_2	TeO_2
Fe_2O_3	$BaTiO_3$
Al_2O_3	CaO

II.1.2. Doping of metal oxides

Doping improves the electrical properties, such as the charge carrier concentration and the electrical conductivity. Substitution, vacancy generation or introduction as interstitials may be affected, depending on the material and the type of doping. By doping it on either side, new donor and acceptor levels can be introduced into the energy gap formed by the conduction and valence bands. There are primarily two types of doped (i) **n-Type doping** and (ii) **p-Type doping** [10].

a) n-Type doping: A pseudo-energy level is produced slightly below the conduction band by the addition of electron donor atoms (figure I.2). Compared to an intrinsic semiconductor, this drastically lowers the energy needed for electrons to move into the conduction band. Creating an excess of free electrons to act as charge carriers in the semiconductor is the primary goal of this technique. Usually, this doping is accomplished by adding oxygen or metal atoms to the material's structure.

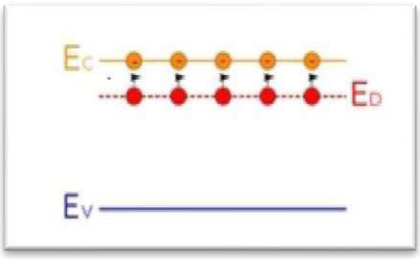


Figure I.2. Representation of the energy level of the doping element (n-type).

b) p-Type doping: Beyond the valence band, a pseudo-energy level is created by the addition of electron acceptor atoms. Valence electrons can migrate to this acceptor level with comparatively little energy. The valence band develops holes as a result of this electron migration. The main objective is to create too many holes, as figure I.3 shows.

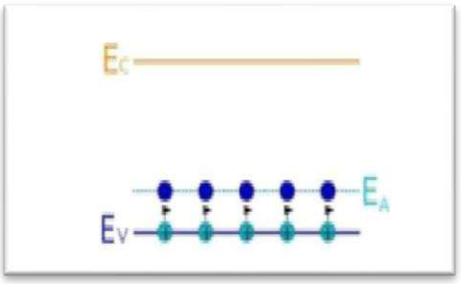


Figure I.3. Representation of the energy level of the doping element (p-type).

III.1. Zinc oxide (ZnO)

Zinc oxide (ZnO) is found naturally in the Earth's crust as Zincite, a substantial crystal (figure I.4 –a-). It possesses an extensive history of research about its growing procedures and material property characterization, with studies originating in 1912.

ZnO is an inorganic chemical, commonly encountered as a white powder that is nearly insoluble in water. This powder is widely utilized as an additive in diverse materials, including ceramics, glass, cement, rubber (notably in automotive tires), lubricants, paints, adhesives, sealants, pigments, food (as a zinc source), batteries, fire retardants, and others; the majority of commercially available ZnO is synthetically manufactured [12, 13].

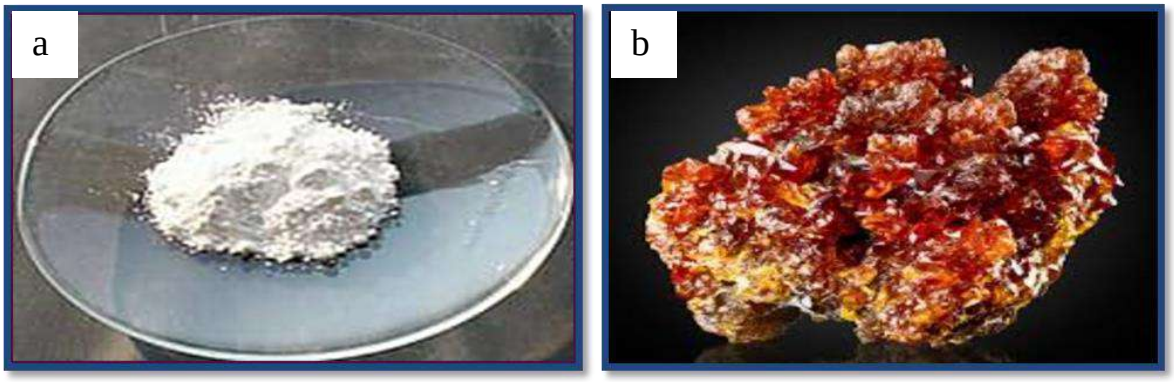


Figure I.4. a) Zinc oxide Powder [14] and b) Photograph of a natural crystal of Zincite [15].

III.1.1. Properties of ZnO

A. Structural properties of ZnO

Zinc oxide crystallizes into three distinct crystallographic phases, as depicted in (Figure I.6), contingent upon the preparation conditions: the cubic rocksalt structure (NaCl), the hexagonal Wurtzite structure, and the zinc blende structure [7].

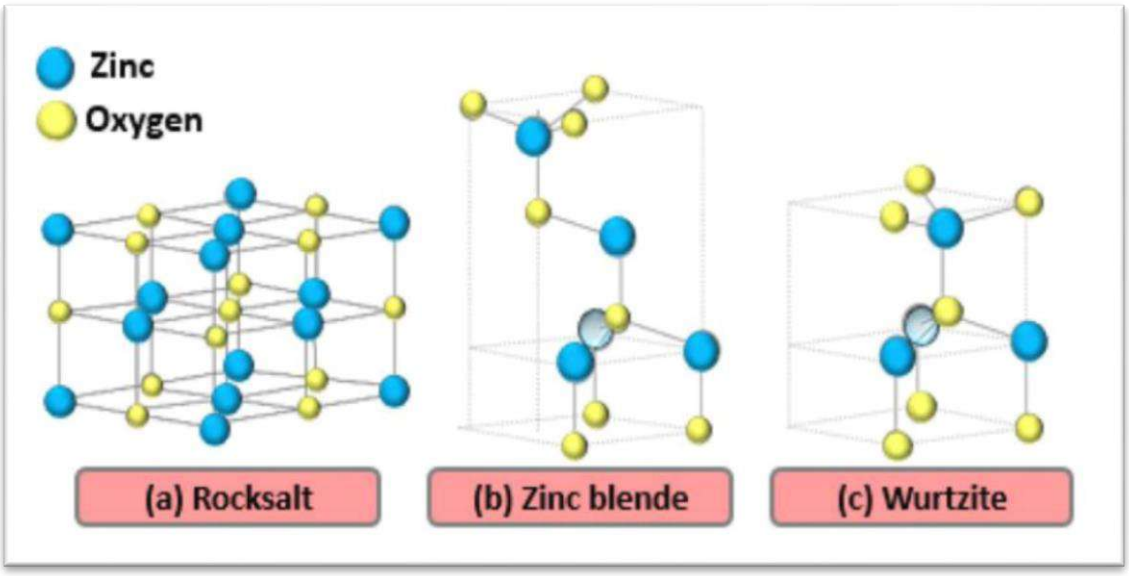


Figure I.5. Crystal structures of ZnO: a) rocksalt, b) zinc blende and c) wurtzite [16].

The blende structure forms when ZnO is deposited on substrates with cubic symmetry, while the rocksalt structure is observed under very high pressures (~10GPa). The thermodynamically stable structure at room temperature is the hexagonal ***Wurtzite*** structure [6]. (Table I.4) presents some properties of the ***Wurtzite*** structure of ZnO.

Table I.3. Some properties of ZnO in the wurtzite structure [7, 17].

Properties	Parameters (Value) at 300 K
Crystalline structure	Wurtzite
Lattice parameters	a=b=3.249 Å / c=5.2042 Å
band gap energy	3.37 eV, direct
Melting point	1975 °C
Density (g/cm³)	5.606
Electron effective mass	0.28 m_o

The hexagonal unit cell of the Wurtzite structure is formed by interpenetrating sub-lattices of O^{2-} anions and Zn^{2+} cations, each containing four atoms of the same type (Figure I.7). The Wurtzite structure is characterized by the stacking of zinc (Zn) and oxygen (O)

atomic planes in an AaBbA pattern. Its unit cell is prismatic and consists of a motif of four atoms [16]:

- Two Zn atoms are located at the coordinates (0, 0, 0) and (1/3, 2/3, 1/2).

- Two O atoms are positioned at (0, 0, 3/8) and (1/3, 2/3, 7/8).

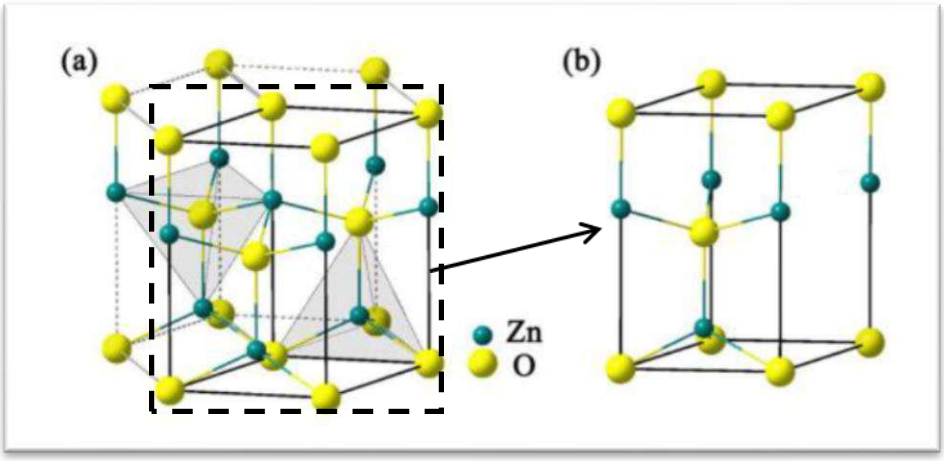


Figure I.6. (a) Wurtzite structure of ZnO and **(b)** Wurtzite unit cell of ZnO [18].

B. Optical properties of ZnO

Zinc oxide is a transparent material in the visible spectrum, exhibiting high transmittance (T > 80%). The refractive index (n) of bulk ZnO is approximately 2 in thin films; the refractive index and absorption coefficient depend on the conditions under which the thin layers are fabricated, with n typically ranging from 1.7 to 2.2. Additionally, ZnO possesses an exceptionally high exciton binding energy of 60 meV, significantly exceeding the thermal energy of 26 meV at room temperature. For the use of zinc oxide in various applications, several authors have studied its various optical properties such as transmission, absorption, reflection, optical gap, and photoluminescence. The research results show that its optical property is related to several parameters that we quote the thickness, the optical gap, the surface roughness, the doping, the crystalline quality of the film, and the deposition method [7, 13].

C. Electrical properties of ZnO

ZnO is a semiconductor belonging to the II-VI group. The electronic structure of zinc (Zn) and oxygen (O) atoms are as follows:

Oxygen (O): $1s^2\ 2s^2\ 2p^4$

Zinc (Zn): $1s^2\ 2s^2\ 2p^6\ 3s^2\ 3p^6\ 4s^2\ 3d^{10}$

Production of quality p-type ZnO films has been problematic, mostly due to defects caused by dopants induced stresses in the crystal. Very low formation energies for oxygen vacancies and zinc interstitials in ZnO have been calculated and likely explain the native n-type conductivity observed in as-grown films [13].

The electrical properties of ZnO thin films (Table I.5), such as: electrical resistivity, charge carrier concentration, and mobility are determined by ***Hall Effect*** measurements. The electrical resistivity (ρ) of an n-type thin film depends on the electron density (n) in the conduction band and their mobility (μ_n), where $\boldsymbol{e}_n$ is the electron charge [12]:

$$\boldsymbol{\sigma = \frac{1}{\rho} = e_n \mu_n} \qquad \textbf{(I.1)}$$

The literature indicates, “If an oxygen vacancy is created in a perfect crystal, two electrons are created in the crystal and contributed as ionized donors”. But, if there is too much oxygen created in the thin films, sub-oxides will form, causing the resistivity to rise.” In addition to the oxygen vacancies, doping (most used dopants are Al, Ga, In, B, Si, Ge, F) also can change the electrical conductivity of ZnO. As host cations are substituted by elements with a valence higher than that of the host, the extra electrons can become conduction electrons. To avoid the charge neutrality, substitution of a higher valence element creates extra electrons. It is well known that pure zinc oxide films usually have a characteristic high resistivity due to their low carrier concentration. Therefore, in order to decrease resistivity, we can increase either the carrier concentration or the carrier mobility in zinc oxide thin films. The former is probably obtained by oxygen and or zinc non-stoichiometry, or doping with an impurity [13].

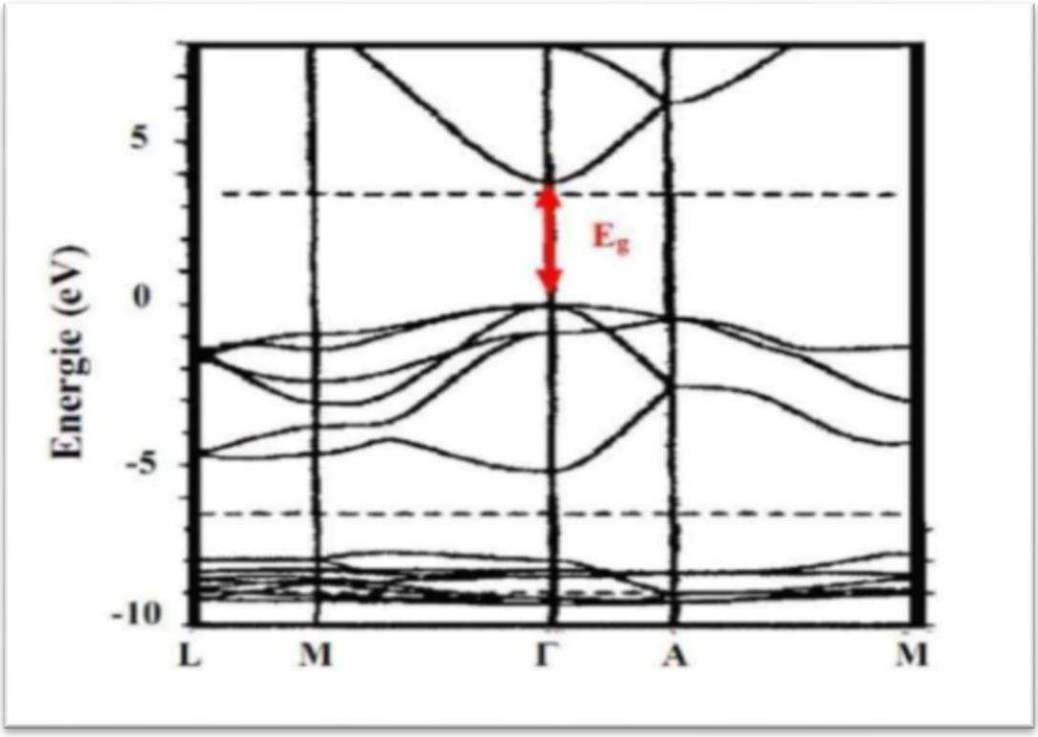


Figure I.7. ZnO band structure [19].

Table I.4. Some electrical properties of ZnO [10].

Nature of the forbidden band	Direct
Band gap width at 300K (eV)	3.34±0.02
Conductivity type	n
Maximum electron mobility ($cm^2/V.s$)	200
Effective mass of electrons	$0.28m_0$
Effective mass of holes	$0.60\ m_0$
State density in BC (cm^3)	3.71×10^{18}
State density in BV (cm^3)	1.16×10^{19}
Electrical resistivity (Ω.cm)	$10^{-1}/10^{6}$

III.1.2. The dopants of ZnO

In general, semiconductors like ZnO, GaN, ZnS, and ZnSe are easily n-doped but are very challenging to p-doped .Undoped ZnO is naturally an n-type semiconductor. Achieving p-type doping in ZnO remains a significant challenge and is considered a key

factor for advancing ZnO-based devices [20].In the following table (Table I.6) the elements that give us the n-type and p-type of ZnO.

Table I.5. The dopants of ZnO [10].

n-type		p-type	
Group III	**Group VII**	**Group I**	**Group V**
Al, Ga, In - Substitution on Zn sites.	Cl, I - Substitution on O sites.	Li, Na, K, Cu, Ag - Vacancies on Zn sites	N, P, As - Vacancies on O sites

III.1.3. Applications of ZnO thin films

The application of ZnO in thin film form has gained prominence in contemporary technology, encompassing several domains including electronics, optics, chemistry, and mechanics. ZnO thin films occupy a prominent role owing to their diverse applications, several of which are detailed below [8]:

- **Electronics and Photovoltaics:** ZnO thin films serve as transparent electrical contacts in thin-film solar cells composed of amorphous or microcrystalline silicon, in addition to photovoltaic solar cells. They are also employed in electronic devices such as varistors, rectifiers, and filters. Moreover, ZnO thin films are utilized in telecommunications as resonators for radio communications, in image processing, and in surface acoustic wave devices.
- **Optics:** Integrated optical waveguides take advantage of ZnO thin-film optical characteristics. These films are also employed in the manufacture of UV photodetectors. In such circumstances, the layers are commonly doped with aluminum, and upon exposure to adequate monochromatic light (350 nm), a photocurrent is created.
- **Piezoelectric Applications:** Due to their piezoelectric properties, ZnO thin films are used as pressure sensors.
- **Gas Sensing:** ZnO thin films possess chemical properties which make them ideal for use as gas sensors. For instance, they can detect methane, an extremely flammable and explosive gas that can be quite perilous when mixed with air. It is also 20 times more harmful than CO_2 and its monitoring in the environment and in the atmosphere is becoming increasingly important properties pointing to the fact that its detection in the ambient is an active field of study.

III.2. Titanium dioxide (TiO_2)

Titanium dioxide (TiO_2) was first identified in the early 1900s, and the production of titanium white, used as a pigment in its anatase form, was first documented in France in 1923. By the early 1930s, it had largely replaced lithopone and toxic lead-based pigments [21].

III.2.1. Properties of TiO_2

A. Structural properties of TiO_2

TiO_2 exists in three crystalline polymorphs (Figure I.9): rutile, anatase, and brookite. Among these, rutile is the thermodynamically most stable phase and has the lowest surface energy, while anatase is more stable at lower temperatures. Brookite, being challenging to synthesize, has limited practical applications. The metastable anatase and brookite phases undergo an irreversible transformation to the rutile phase when heated to temperatures between 600°C and 800°C [13].

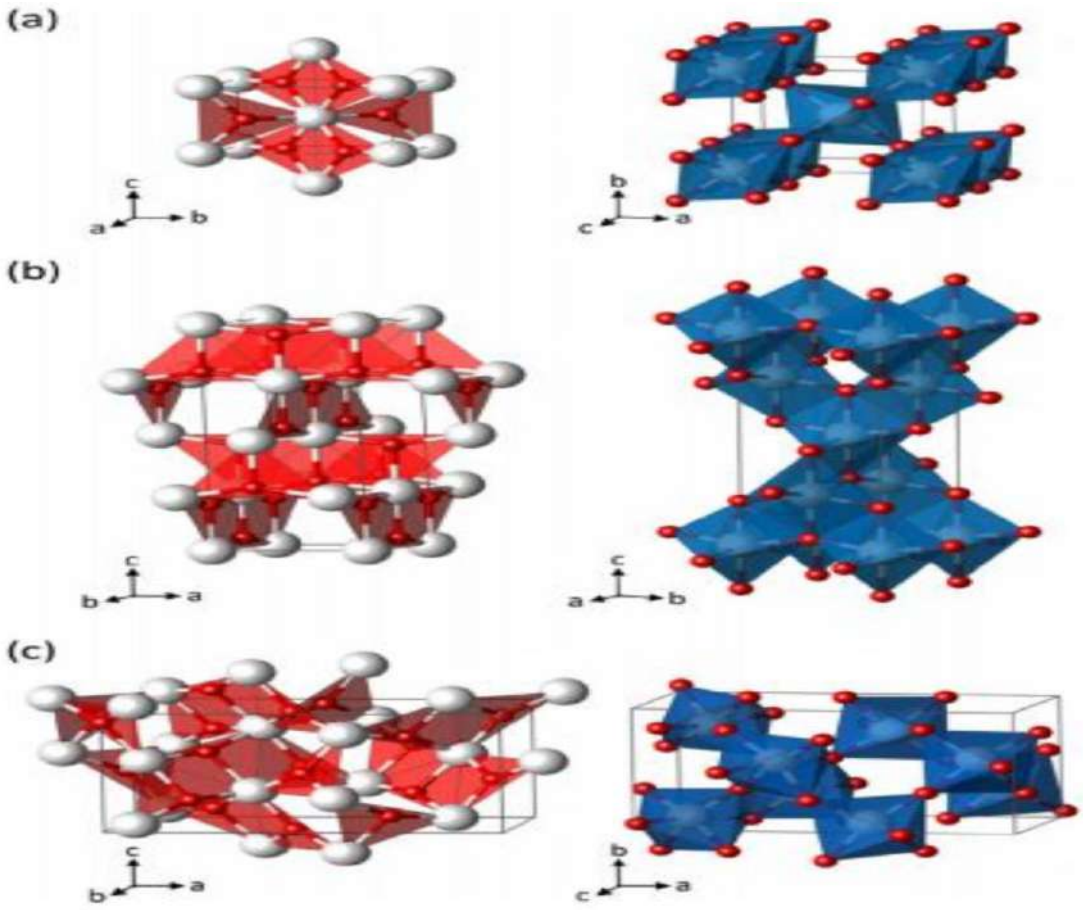


Figure I.8. Planar Ti_3O building-block representation (left) and TiO_6 polyhedra (right) for the TiO_2 phases rutile (a), anatase (b) and brookite (c) (Ti (white); O (red)) [22].

Table I.6. Crystal structure data of TiO_2 [23].

Phase	Rutile	Anatase	Brookite
Crystal structure	Tetragonal	Tetragonal	Orthorhombic
Lettice constants (Å)	a=4.5936 c=2.9587	a=3.784 c=9.515	a=9.184 b=5.447 c=5.145
Molecule/cell	2	4	8
Volume/molecule (Å³)	31.2160	34.061	32.172
Density (g/cm³)	4.13	3.79	3.99
Ti–O bond length (Å)	1.949 (4) 1.980 (2)	1.937 (4) 1.965 (2)	1.87~2.04
O–Ti–O bond angle	81.2° 90°	77.7° 92.6°	77°~105°

B. Optical properties of TiO_2

The primary use of titanium dioxide is attributed to its excellent optical properties, which stem from its high refractive index and transparency in the visible range. Significant differences between the TiO_2 structures are observed in their high refractive indices, with values as follows: rutile (2.605–2.903), anatase (2.561–2.488), and brookite (2.583–2.700). The band gap of anatase is indirect, but rutile and brookite are direct with values of 3.23 eV, 3.02 eV, and 3.10 eV, respectively. TiO_2 is a favored material in the field of photonic crystals due to its wide band gap and high refractive index. It is an excellent photocatalyst for solar energy conversion in the UV range. Thin-film TiO_2 is widely used in most optical treatments, including anti-reflective coatings for ophthalmic lenses and interference filters for optical telecommunication applications. The reduction in porosity with annealing temperature has been confirmed by the work of ***Negishi*** and ***Takeuchi*** [24].

C. Electrical properties of TiO_2

Titanium dioxide is n-type semiconductor. The TiO_2 single crystal has a resistivity about 10^{13} Ω.cm at room temperature and about 10^{7}Ω.cm at 250°C. These values are similar to reported conductivity for a rutile single crystal at 30 °C which was about 5.10^{-14} $\Omega^{-1}.cm^{-1}$. While at 260°C it was decreased to 3.3×10^{-9} $\Omega^{-1}.cm^{-1}$. Therefore, TiO_2 is generally considered as an insulator for temperatures below 200 °C and it was used for diversity applications such as a dielectric gate in MOSFET devices. However, the electrical properties of the TiO_2 films can be modified to become very conductive for many applications such as: gas sensors, photocatalyst and solar cells contact (Figure I.10) depicts TiO_2 band structure as can be seen

TiO_2 is a wide band-gap semiconductor material. The gaps of Rutile, Anatase and Brookite have a value of 3 eV, 3.2 eV and 3.1 eV respectively .These gap values give rise to transitions corresponding to photons in the ultraviolet range [13].

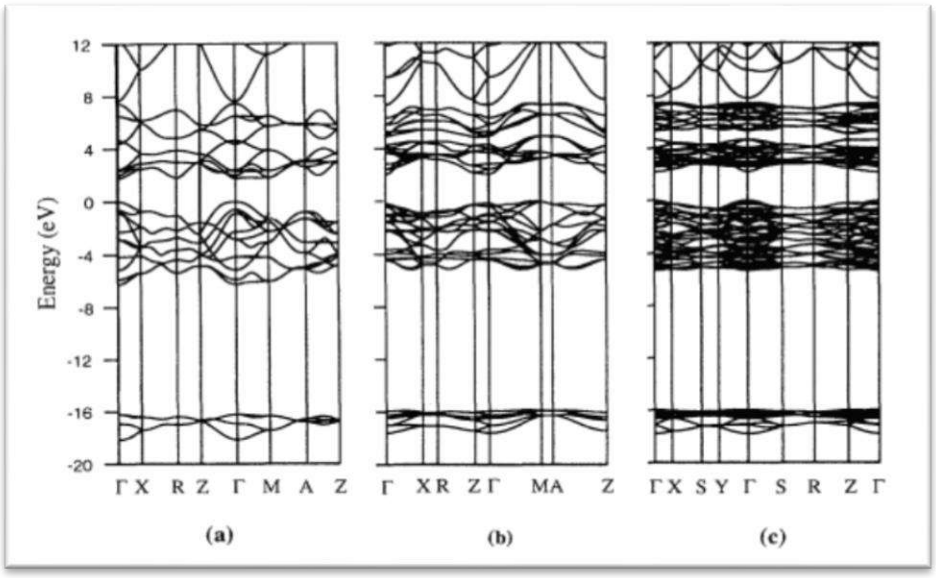


Figure I.9. TiO_2 band structure for rutile (a), anatase (b) and brookite (c) [23].

IV.1 Overview on thin film

IV.1.1. General concept of thin films

A thin film of a material is a form of that material where one dimension, known as the thickness, has been significantly reduced to the micrometer scale. This reduction results in a quasi-two-dimensional structure, which in turn alters many of the material's physical properties. The key distinction between a material in its bulk form and as a thin film lies in the influence of boundaries. In bulk materials, boundary effects are typically negligible, whereas in thin films, these surface-related effects dominate. The thinner the film, the more pronounced these two-dimensional effects become. Conversely, when the film's thickness surpasses a certain threshold, these effects diminish, and the material's properties begin to resemble those of its bulk counterpart [25].

IV.1.2. Principal of thin films deposition

In the thin film deposition process, following basic steps are to be considered [26].

- The initial materials used for the deposition is prepared in the atomic, molecular or finest particulate form before the deposition;

- ❖ The finest form of materials is transported on the substrate in the form of vapor stream, the solid, or the spray;
- ❖ Deposition of the material on the substrate and the film growth by nucleation-growth process.

IV.1.3. Classification of thin films deposition techniques

The thin film materials are obtained by different ways of deposition; deposition methods are roughly divided in two categories, chemical vapor deposition (CVD) and physical vapor deposition (PVD) (Figure I.11).

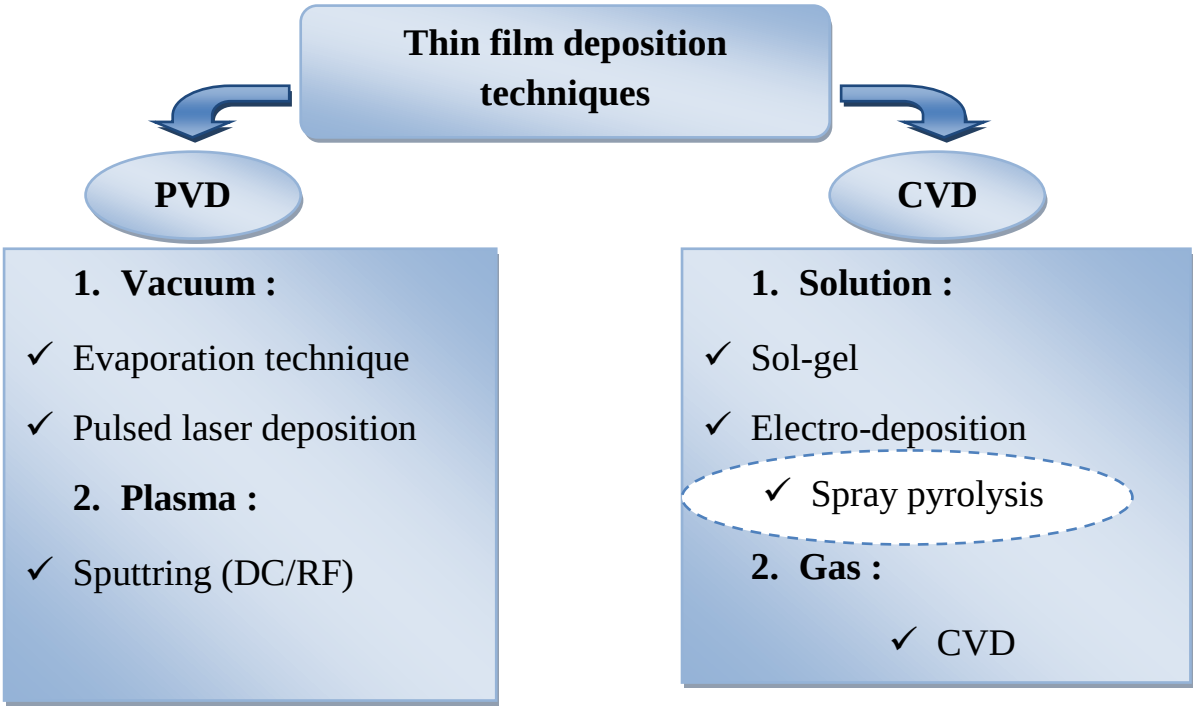


Figure I.11. Classification of thin film deposition technique.

IV.1.3.1. Physical deposition techniques

The physical deposition techniques are those in which the material required for deposition is made available in the atomic, molecular or particulate form before deposition. This is usually done at sufficiently high temperature. The condensation of vapor on substrate material kept at relatively low temperature yields [26]. Physical deposition can be further subdivided in:

1. **In vacuum**

   i. **Evaporation techniques**

Evaporation methods are considered as the common deposition of materials in the form of thin-layer films. The general mechanism of these methods is obtained by changing the phase of the material from solid phase to vapor phase and converting again to solid phase on the specific substrate. It takes place under vacuum or controlled atmospheric condition.

a. Vacuum thermal evaporation technique

Vacuum evaporation technique is one of the oldest and extensively used method for semiconducting thin film deposition at industrial scale. It is a simplest technique for synthesis of amorphous film especially chalcogenide films such as CdSSe, MnS, Ge-Te-Ga, and used to protect textiles from metal nanoparticles deposition. The vacuum helps to settle vapors of coating particles on the substrate where it converts back into the solid phase. The evaporation is carried out by electron beam heating or electrical heating. The technique of thermal evaporation is strongly dependent on two parameters: thermally vaporized material and applying a potential difference to the substrate under medium or higher vacuum level ranging from 10^{-5} to 10^{-9} mbar [27]. Figure I.12 shows the schematic diagram of vacuum thermal evaporation technique.

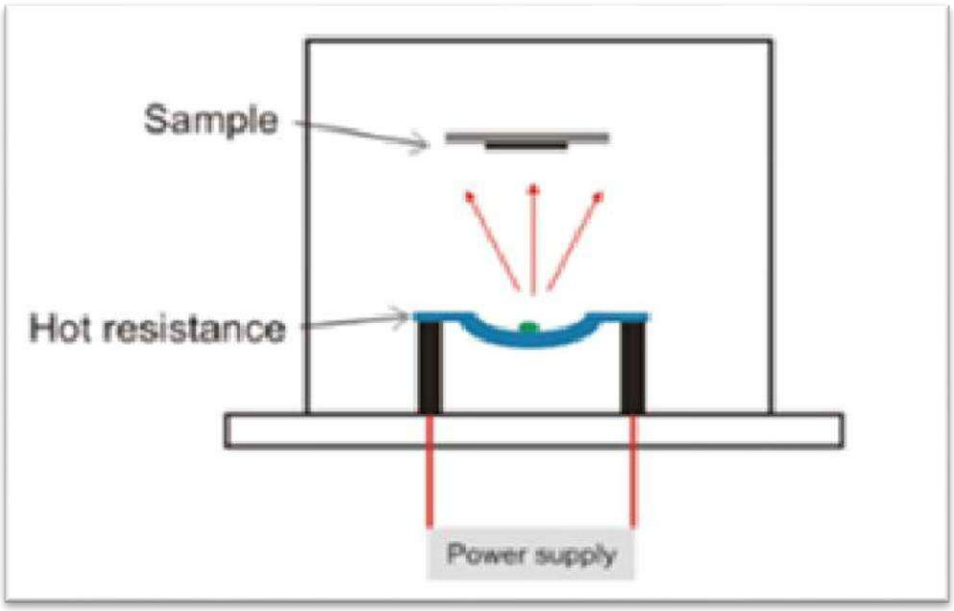


Figure I.12. Schematic of Vacuum thermal evaporation technique [27].

b. Electron beam evaporation

This type of evaporation is another method of physical deposition where the intensive beam of electrons is generated from a filament and steered through both electric and magnetic fields to hit the target and vaporize it under vacuum environment as shown in (Figure I.13) thin films prepared by electron beam evaporation are of good quality and purity [28].

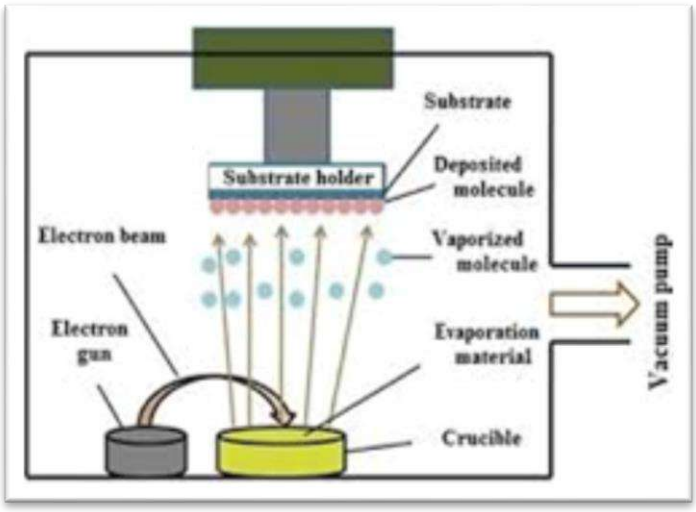


Figure I.13. Schematic diagram of electron beam evaporation [28].

ii. Pulsed-laser deposition

For physical depositions, PLD requires lenses to focus the laser beam, in order to focus large energy density to ablate the target source and the vaporized materials eventually sublimate on the substrates. PLD is a clean and simple method to obtain a wide range of structures, compositions, and properties [29].

During the thin-film deposition process, the laser beam is used to ablate the material for depositing the thin films inside a vacuum chamber as shown in (Figure I.14). When the laser beam strikes the target material, it produces the plume, which could deposit on the various substrates. The created plume may contain neural- and ground-state atoms and ionized species. Different kinds of laser sources are being used to ablate the target. The most common sources are KrF (248 nm), XeCl (308 nm), and Nd-YAG laser (1064 nm) .In the case of metal oxide thin films, oxygen is used to deposit the oxides metals. The coating of thin films through PLD follows three modes: Frank–van der Merwe, Volmer–Weber, and Stranski–Krastanov. PLD has some advantages over other physical deposition. Among them are the availability of less space for the board and the availability of software design [27].

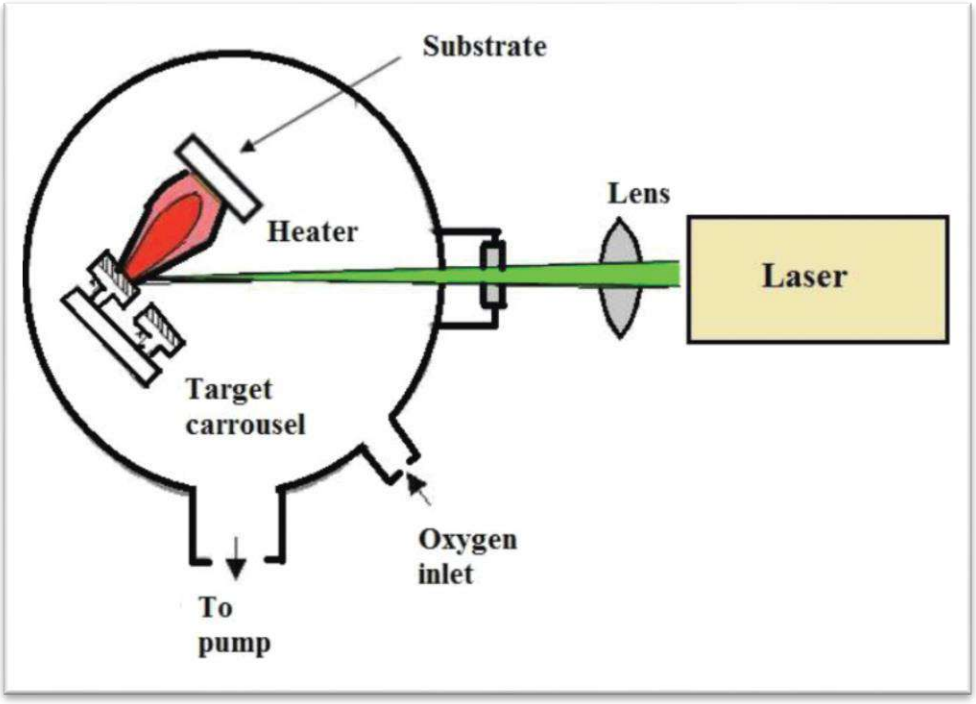


Figure I.14. General diagram of PLD [28].

2. In plasma

a) Sputtering technique

Sputtering is another physical vapor deposition process occurs in a vacuum chamber. A large piece of the material to deposited, known as a target, is bombarded with high energy argon ions from a glow discharge. When the argon ions strike the target, they knock off target atoms and molecules, which are then conveyed through the vacuum to the substrate, where they condense and form a thin film. Sputtering is most commonly used for depositing metal films, but, like evaporation, can also deposit insulating films with some slight process and equipment variations. There are many other types of sputtering are: Magnetron Sputtering, Reactive Sputtering, and Ion Beam Sputtering.

It has several advantages, high-melting point materials can be easily formed by sputtering.The deposited films have composition similar to the composition of the starting materials .The general sputtering method can be used to prepare a variety of materials such as metals, semiconductors, insulators, etc., and has the advantages of simple equipment, easy control, large coating area, and strong adhesion [27] . The diagram of the sputtering system is shown in (Figure I.15).

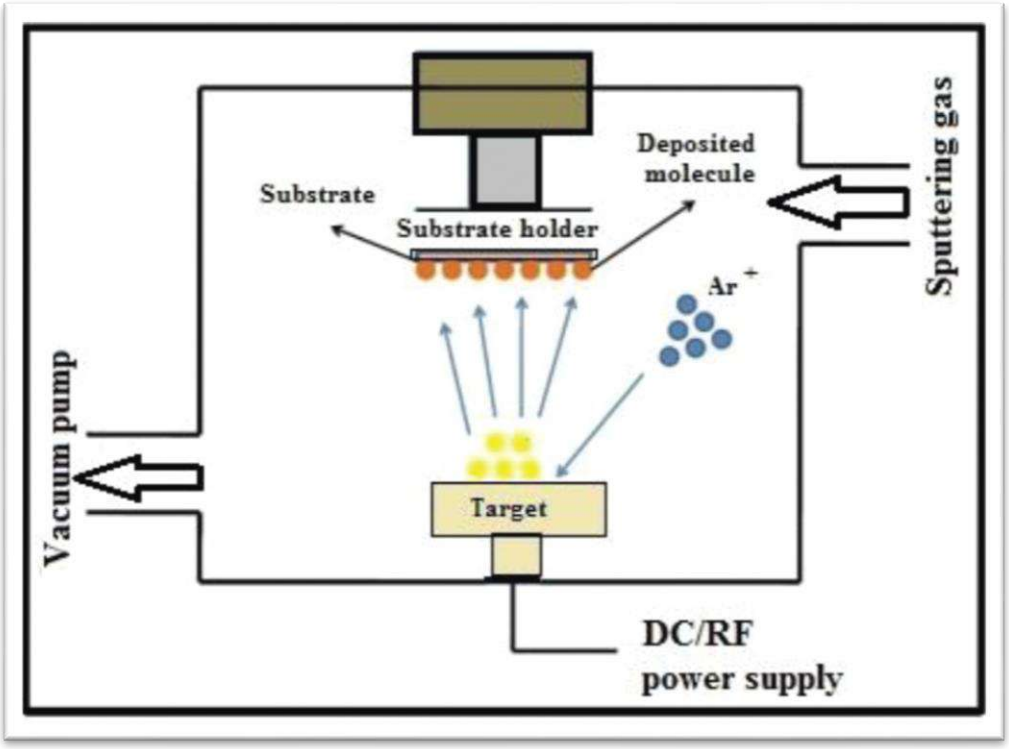


Figure I.15. Sputtering system diagram [28].

IV.1.3.2. Chemical deposition techniques

1. In solution

a. Sol-gel technique

The sol-gel process is regarded as being a cost-effective and simple technique to synthesize primarily oxide ceramicsThe sol-gel technique is broadly used for the synthesis of oxide materials (Figure I.16). Sol-gel process is one of the famous wet-chemical methods. It works under lower-temperature processing and gives better homogeneity for multicomponent materials. The word 'sol' means the formation of a colloidal suspension and 'gel' means the conversion of 'sol' to viscous gels or solid materials. Two routes are used to prepare transition metal oxides (TMOs) as follows [26]:

- ✓ Preparing of inorganic precursors via inorganic salts in aqueous solution.
- ✓ Preparing of metal alkoxide precursors via metal alkoxides in no aqueous solvents.

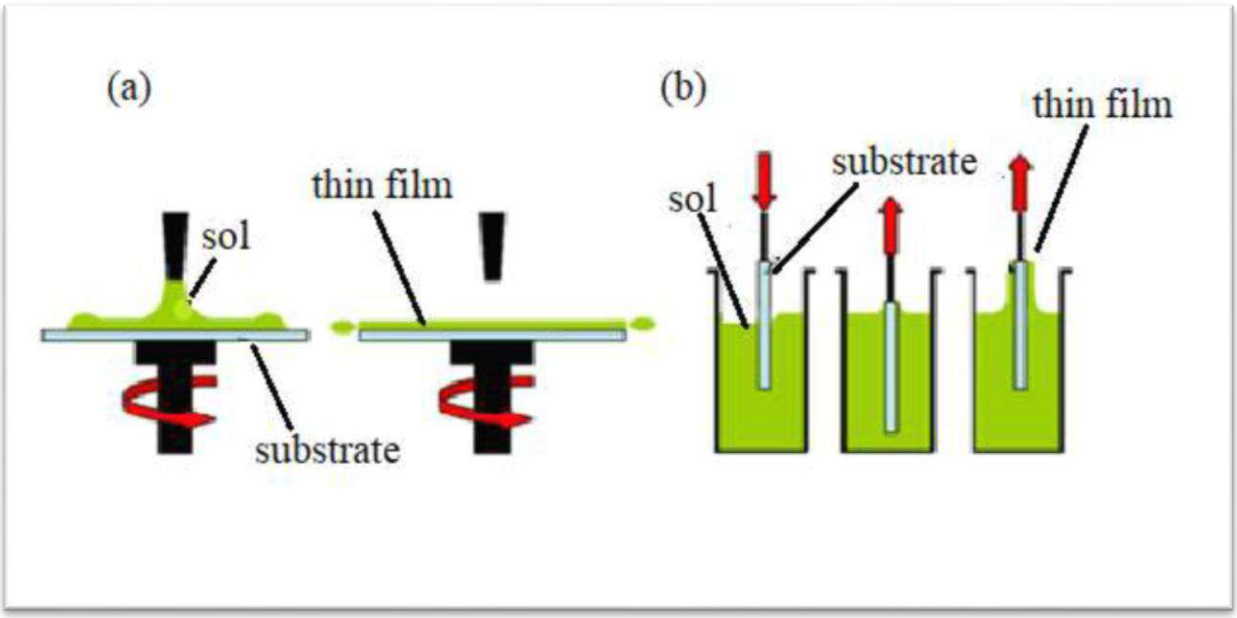


Figure I.16. Sol-gel process diagram (a): Spin-coating, (b): Dip-coating [27].

b. Spray Pyrolysis technique

The spray pyrolysis technique was initially introduced by ***Chamberlin*** and ***Skarman*** in 1963. It was effectively employed for the deposition of CdS thin films and subsequently modified for the synthesis of various materials, including Cd, Zn, Sn, $CuInS_2$, FeS_2, among others, as well as for the fabrication of transparent conductive oxide (TCO) thin films (SnO_2, ZnO, NiO). The spray pyrolysis method entails atomizing a precursor solution containing the constituent atoms of the target compound onto a heated substrate. The substrate temperature promotes the activation of chemical reactions among the volatile components of the solution at the surface. These volatile byproducts are promptly removed, resulting in the formation of the synthesized compound as a thin film.

"Spray Pyrolysis" is the most widely used name for this technique. It combines two components: "spray" and "pyrolysis":

- **"Spray":** Refers to the English term for atomizing a liquid into fine droplets using a spray nozzle or atomizer.

- **"Pyrolysis":** Derived from the term "pyrolytic", it denotes the heating of the substrate. This step triggers the thermal decomposition of a precursor source, releasing a metal or compound to form the desired material.

Spray Pyrolysis is a highly suitable method for preparing thin films with thicknesses ranging from tens to several hundreds of nanometers. For instance, various ZnO thin films have been successfully synthesized using this technique. In this process, inexpensive precursors such as nitrates, chlorides, and acetates are typically dissolved in a solvent medium, which may include distilled water, methanol, or a methanol-water mixture [30].

A straightforward and inexpensive method based on the chemical vapor deposition process (CVD) is spray pyrolysis. Using air as a carrier gas, the precursor of the material to be deposited is sprayed onto a heated substrate while in solution. There are numerous deposition factors (process parameters) in the spray pyrolysis technique, including substrate temperature, gas and solution flow rates, the precursor's concentration and composition in the starting solution, deposition time, substrate-nozzle distance, etc. There are several of these characteristics that depend on one another. However, the other ones must be held constant in order to examine the impacts of any one of these [13]. Figure I.17 shows the spray pyrolysis technique.

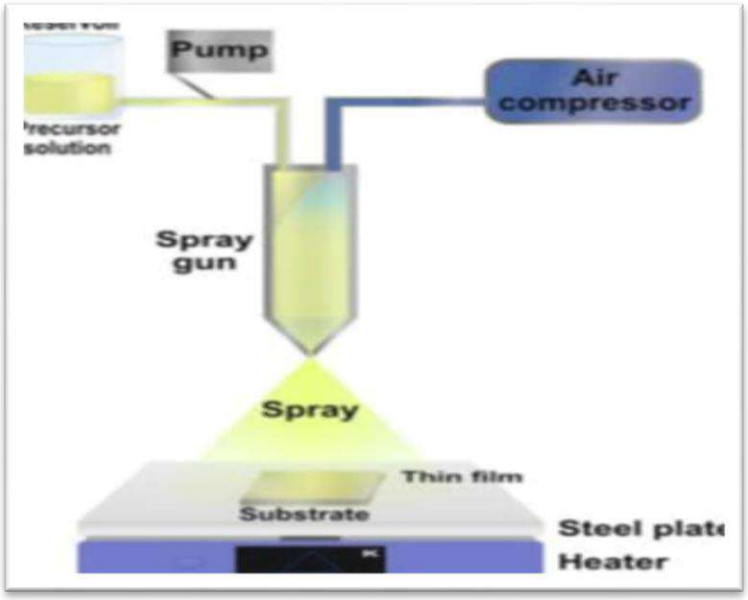


Figure I.17. Shows the spray pyrolysis technique [27].

Chapter II

Elaboration technique and characterization tools



Part One: elaboration of thin films

II.1 Preparation of substrate

II.1.1. Choice of substrate

The studied films were deposited on solid glass substrates; this deposition substrate was chosen for the following reasons [13]:

- The thermal compatibility with TiO_2 and ZnO (thermal dilation coefficients is $\alpha_{glass} = 3.3 \times 10^{-6}K^{-1}$, $\alpha_{TiO2} = 8{-}10 \times (10^{-6}K^{-1})$ and $\alpha_{ZnO} = 3.9{\times}10^{-6}K^{-1}$) which minimize the stress in the interface film/substrate,
- For their transparency which adapts well for the optical characterization of films in the visible one,
- For economic reasons.

II.1.2. Cleaning the substrates

After using a diamond pen to cut substrates (Figure II.1) with a length of ~ 2.5 *cm* and a width of ~ 2.5 *cm*, the purity and surface condition are the main factors in the adhesion and quality of thin films.



Figure II.1. Glasses substrates.

Therefore, the method for cleaning the surface of substrates is as follows:

1) Cleaning with a soap solution,
2) Rinse with distilled water,
3) Rinse with acetone for 5 minutes,
4) Rinse with ethanol for 5 minutes,
5) Cleaning in a water bath,
6) Drying with optical paper.

II.2 The choice of spray pyrolysis technique

This technique was chosen for several key reasons [31, 16]:

- ❖ Produces uniform thin films with precise thickness over large areas,
- ❖ Fast and simple process, reducing production time,
- ❖ Enables precise chemical composition control, ideal for doping,
- ❖ Yields high-quality films with enhanced light absorption,
- ❖ Cost-effective due to low cost and high throughput,
- ❖ Scalable for large-area industrial applications like solar cells and displays.

II.3. Preparation of solution

This work aims to investigate the effect of mass doping with Aluminum (Al) and interlayer of TiO_2 on the structural and optical characteristics of zinc oxide thin films elaborated by Spray pyrolysis method. The table II.1 below shows the different chemical compounds used to deposit thin films.

Table II.1. Different products used for the preparation of our thin films.

Product	Formula	Mark	Purity (%)
Zinc acetate dihydrate	$Zn(CH_3CO_2)_2.2H_2O$	Aldrich	99
Ethanol	(CH_3CH_2OH)	Biochem	99.9
Isopropanol	$CH_3CHOHCH_3$	Prolabo	98
Aluminium sulfate octadecahydrate	$(Al_2 (SO_4)_3 \cdot 18H_2O)$.	Prolabo	99
Titanium isopropoxide	$Ti [OCH(CH_3)_2]_4$	Aldrich	97

1. For undoped and doped ZnO

To prepare the solutions, we first calculate the mass of zinc acetate (m) using the following equation:

$$m = M.C.V \qquad \text{II.1}$$

where, ***M*:** the molar mass (219.50 g/mol), ***C*:** the molar concentration (0.2 mol/l), ***V*:** the volume of the solvent (30 ml).

We find m=1.317g. This mass is dissolved en 30 ml of ethanol with thorough stirring using a magnetic stirrer, in this way the first solution is obtained.



Figure II.2. The experimental setup used.

Table II.2. The experimental conditions for the spray deposition of thin films.

Substrate temperature (°C)	450
Nozzle-substrate distance (cm)	25
solution concentration (mol/l)	0.2
Deposition time (min)	15

Doping by weight percentage with the aluminum element (5 % wt.) was carried out using an appropriate precursor ($Al_2 (SO_4)_3 \cdot 18H_2O$), which was directly added to the initial solution (comprising ethanol and zinc acetate) with thorough mixing using a magnetic stirrer. Subsequently, the solution was deposited onto glass substrates placed on a heating source at 450°C for 15 minutes (Figure II.2 and Table II.2), using the thermal spraying technique. During this process, the liquid is evenly distributed, leading to the formation of a uniform and porous thin film.

2. For Titanium dioxide (TiO_2)

To prepare the precipitation solution with a concentration of 0.2mol/L, a volume of 1.776 ml of titanium isopropoxide used as the titanium source is mixed with 30 ml of isopropanol. The solution is stirred well using a magnetic stirrer, and then sprayed onto the pre-prepared substrates using the spray pyrolysis technique**.**

The experimental procedure is summarized in the following schematic diagram (figure II.3).

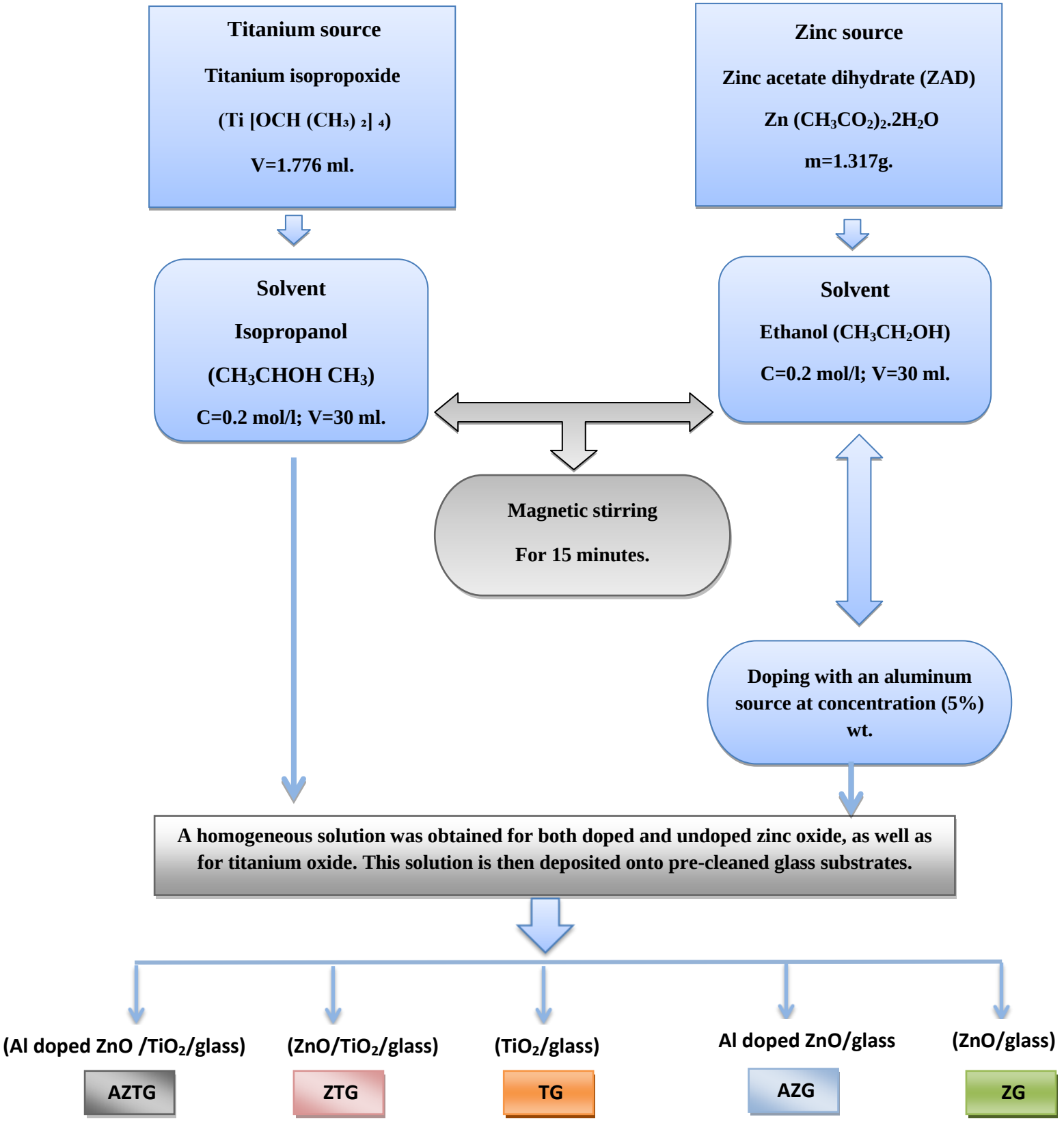


Figure II.3. Schematically represents the preparation steps of thin films using the spray pyrolysis technique.

Part two: Characterization techniques of thin films

II.1. Structural characterization and measurement

II.1.1. Fourier Transform Infrared Spectroscopy (FTIR)

Fourier Transform Infrared Spectroscopy (***FTIR***) is based on the absorption of infrared radiation by the analyzed material. By detecting the characteristic vibrations of chemical bonds, it allows the identification of the chemical functions present in the material. When the wavelength (or energy) delivered by the light beam is close to the vibrational energy of the molecule, the latter absorbs the radiation, leading to a recorded decrease in the intensity of the reflected or transmitted beam. The infrared region from 4000 cm^{-1} to 400 cm^{-1} (2.5 – 25 µm) corresponds to the vibrational energy range of molecules [32].

Not all molecular vibrations result in absorption; this depends on the geometry of the molecule, particularly its symmetry. For a given geometry, the infrared-active vibrational modes can be determined by comparing with frequency tables of common functional groups. These tables allow the assignment of absorption bands to the corresponding chemical groups. The position of these absorption bands mainly depends on the difference in electronegativity between atoms and their masses.

Analyses were carried out using a Fourier Transform spectrometer. It is controlled by a microcomputer and operates in the range of 4000 to 400 cm^{-1}. This analytical technique is simple to implement and non-destructive. It enables the analysis of both organic and inorganic materials. The wide variety of experimental configurations allows for the characterization of almost any type of sample, regardless of their physical state or surface nature:

- Films deposited on an infrared-transparent substrate: transmission mode.
- Films deposited on an infrared-opaque substrate: Attenuated Total Reflectance (ATR) mode.
- Polymer films: transmission mode (if the thickness is less than 10 µm), otherwise ATR mode.
- Powders (dispersed in a KBr pellet): transmission mode.

In our experiment, we used a JASCO FT/IR 4X Fourier Transform Infrared spectrometer (Figure II.4).



Figure II.4. Experimental device for FT-IR spectroscopy (JASCO-4X).

II.2. Optical characterization and measurement

II.2.1. Ultraviolet-visible spectroscopy

Ultraviolet-visible spectroscopy is a non-destructive optical characterization technique (Figure II.5) that relies on the transition of electrons from the ground state to an excited state when exposed to electromagnetic waves. This method enables the analysis of small quantities of materials, either in thin-film form or in suspension. This technique encompasses both absorption and reflectance spectroscopy within the ultraviolet-visible spectral range. The absorption or reflectance in the visible region directly influences the perceived color of the analyzed chemicals. It works by measuring the intensity of light passing through a sample (I) and comparing it to the initial light intensity before interaction with the sample (I_o). The ratio (I/I_o), known as transmittance, is typically expressed as a percentage (T %) [33, 34].

In addition to the previously mentioned capabilities, this technique provides valuable insights into various optical properties, including the optical absorption coefficient (α), the estimation of the optical band gap (E_g), and the optical refractive index (n, k). In certain cases, it can also be used to determine the thickness of the studied sample [35]. In our experiment, we used a JASCO V-730 UV-Visible spectrophotometer (Figure II.6).

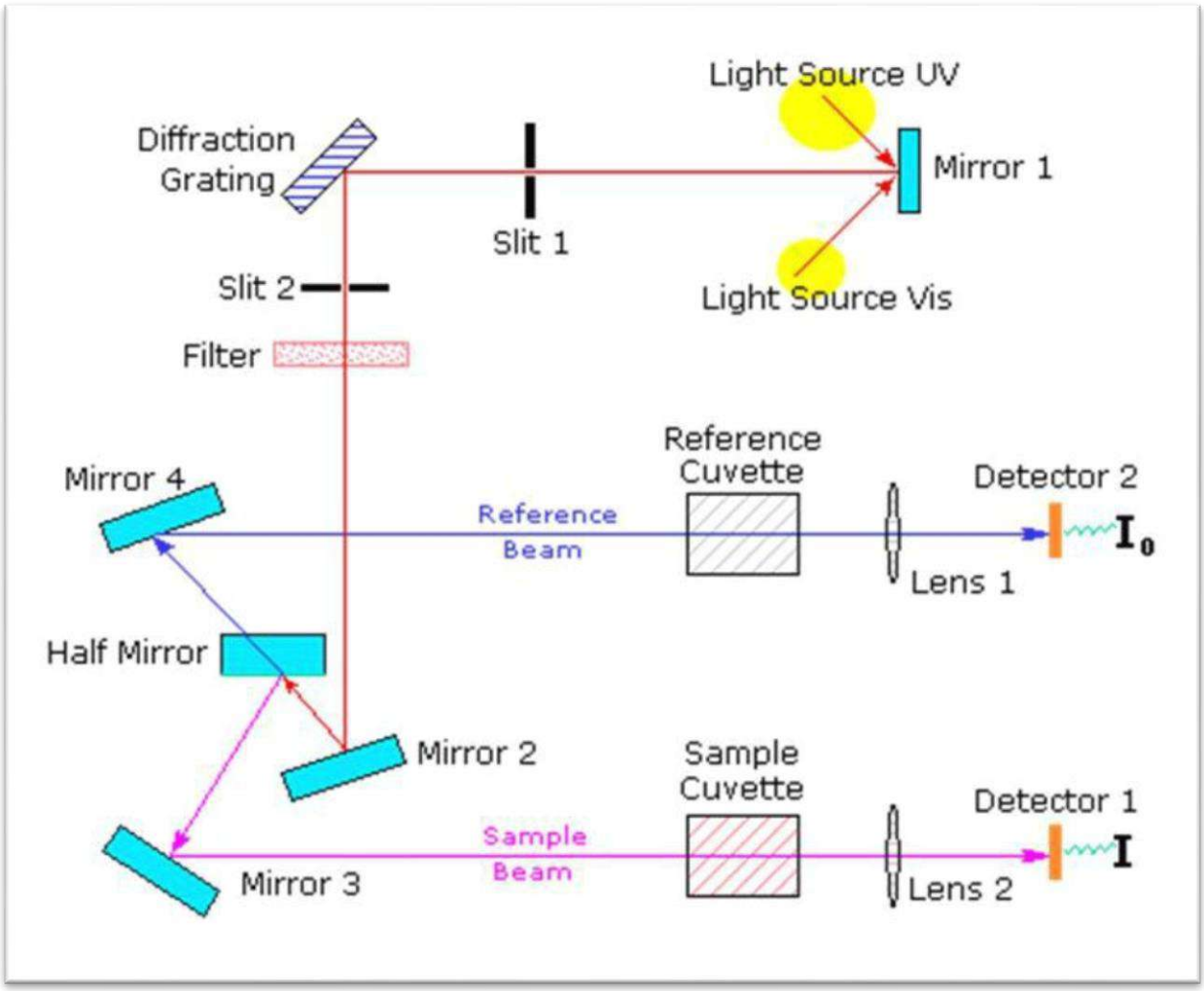


Figure II.5. Schematic spectrometer of UV-Vis [36].



Figure II.6. Experimental device for UV-Vis-NIR spectroscopy (JASCO V-730).

II.2.1.1. Determination of film thickness (d) and refractive index (n)

As previously mentioned, the thickness of a sample can be measured using transmission spectroscopy in the UV-Visible-IR range. The thickness of the layer is determined using the following relation [13]:

$$\mathbf{d} = \frac{\boldsymbol{\lambda_1\lambda_2}}{\mathbf{2(\lambda_1 n_2 - \lambda_2 n_1)}} \qquad \textbf{II.2}$$

λ_1 and λ_2 are the wavelengths of two consecutive maxima (Figure II.7), and n_1 and n_2 are the refractive indices of the layer at wavelengths λ_1 and λ_2. These two indices can be determined using the following relation:

$$\mathbf{n_{1,2}} = [\mathbf{N} + (\mathbf{N^2} - \mathbf{S^2})^{\mathbf{1/2}}]^{1/2} \qquad \textbf{II.3}$$

S: Refractive index of the substrate.

$N_{1,2}$ can be calculated using the following relation:

$$\boldsymbol{N_{1,2}} = \mathbf{2}\boldsymbol{S}[\frac{T_M - T_m}{T_M * T_m}] + (\frac{\boldsymbol{S^2+1}}{\mathbf{2}}) \qquad \textbf{II.4}$$

T_M: Maximum transmission.

T_m: Minimum transmission located between the two maxima.

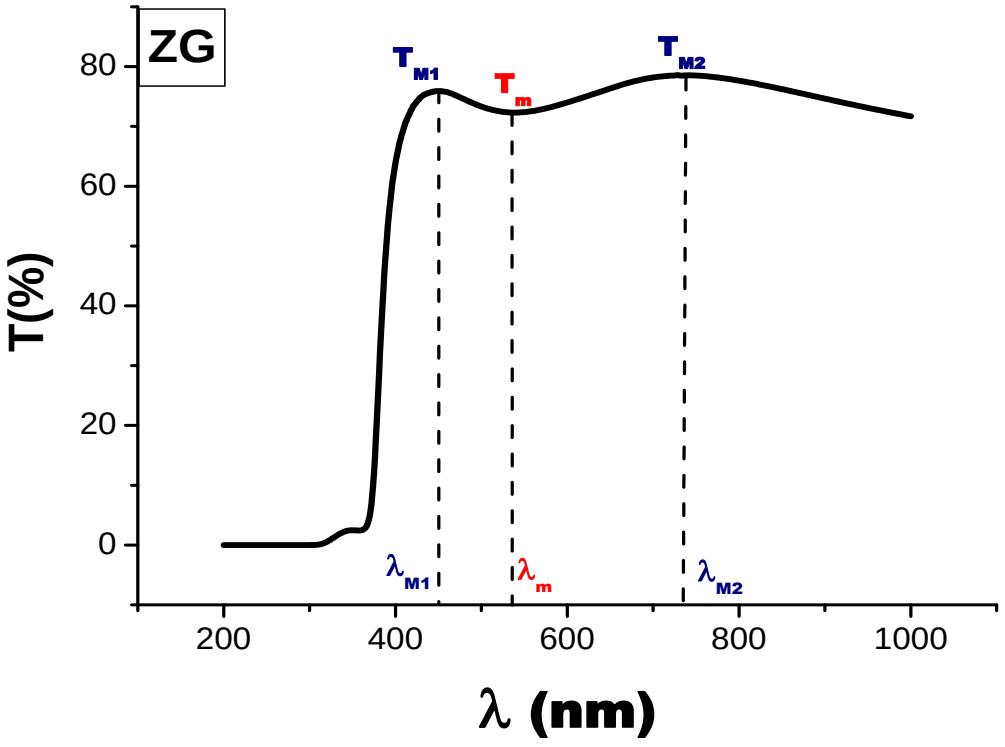


Figure II.7. Determination of interference fringes for find the refractive index and film thickness.

II.2.1.2. Determination of absorption coefficient (α)

When the UV-Visible spectrum passes through the sample, some rays are absorbed by the thin film rather than passing through it, while reflection remains negligible.

In the spectrum domain where light is absorbed and knowing the film thickness (d), the absorption coefficient of the film can be calculated as a function of wavelength using the Beer-Lambert law [37]:

$$T = e^{-\alpha d} \qquad \text{II.5}$$

Where:

$$\alpha = \frac{1}{d} \ln\left(\frac{100}{T(\%)}\right) \qquad \text{II.6}$$

II.2.1.3. Determination of optical band gap (E_g)

The measurement of the optical band gap in materials is essential in the fields of nanomaterial semiconductors and solar energy industries. This note outlines the method for determining a material's optical band gap using its UV-Visible absorption spectrum.

The term "band gap" represents the energy difference between the top of the valence band and the bottom of the conduction band, enabling electron transitions between these bands. For an electron to move from the valence band to the conduction band, it must acquire a minimum amount of energy, referred to as the band gap energy [38].

The optical band gap energy (E_g) for an allowed transition between the conduction and valence bands can be determined using ***Tauc's*** equation II.7:

$$(\alpha h\nu)^n = A(h\nu - Eg) \qquad \text{II.7}$$

Where:

hν: Energy of incident photon (eV),

A: Constant dependent on electron-hole mobility,

E_g: Energy of the optical gap (eV).

n = 2 or **n** = 1/2 following respectively direct or indirect gap transition.

The point of intersection with the horizontal axıs indicates the value of the optical gap. A diagram illustrating the band gap is shown in figure II.8.

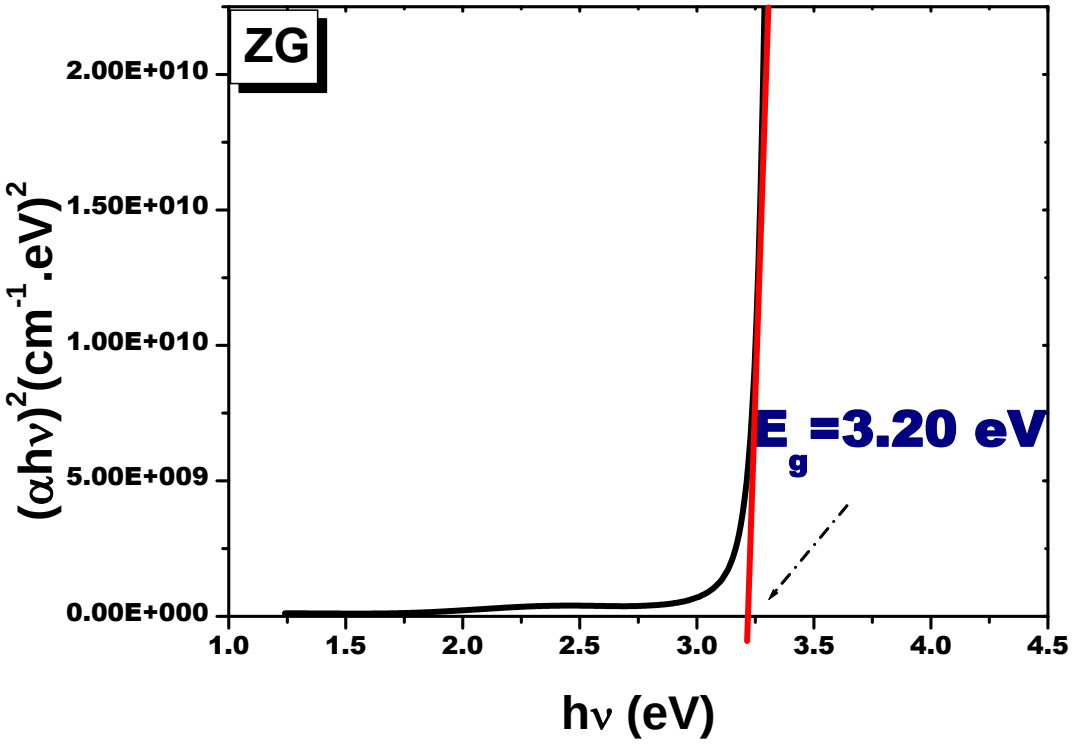


Figure II.8. Determination of optical band gap.

II.2.1.4. Determination of Urbach energy (E_u/E_{00})

Another important parameter that characterizes the disorder of the material is energy of Urbach. According to Urbach's law, the expression of the absorption coefficient is according to the equation II.8 [36].

$$\alpha = \alpha_0 \, exp(\frac{h\nu}{E00}) \qquad \textbf{II.8}$$

Where α_0: Constant, and E_{00}: Energy of Urbach. By plotting (lnα) as a function of hυ (Figure II.9), we can access the value of E_{00}.

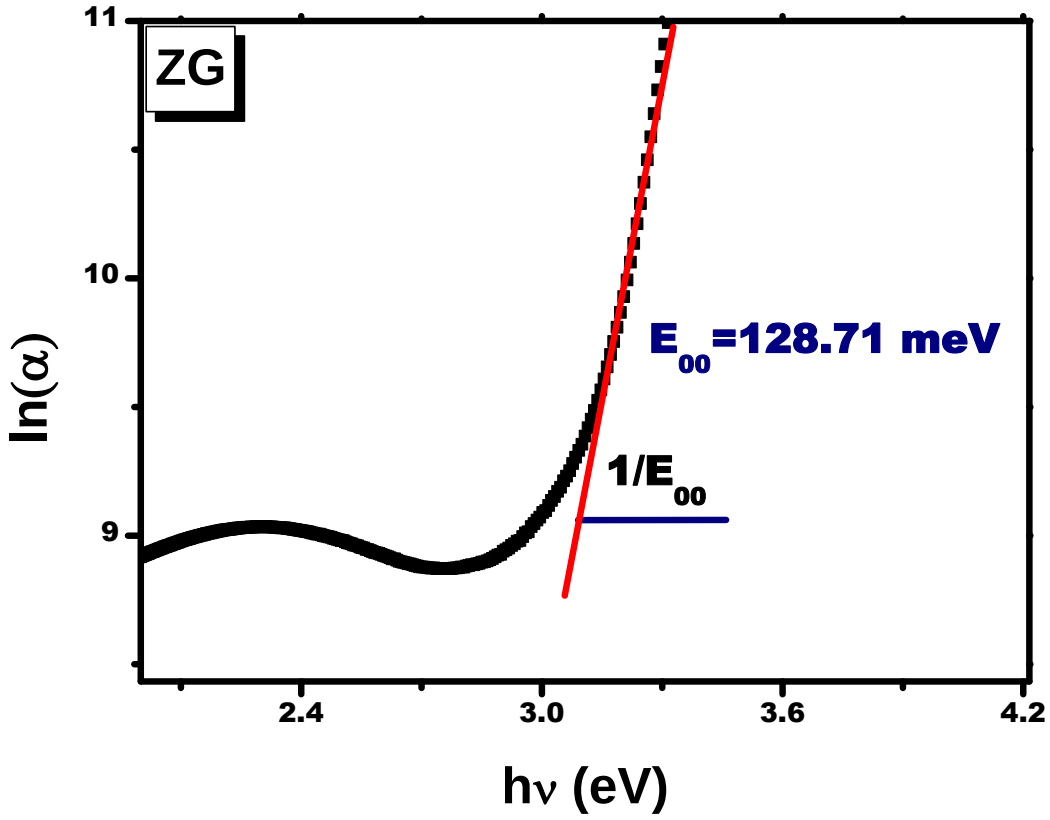
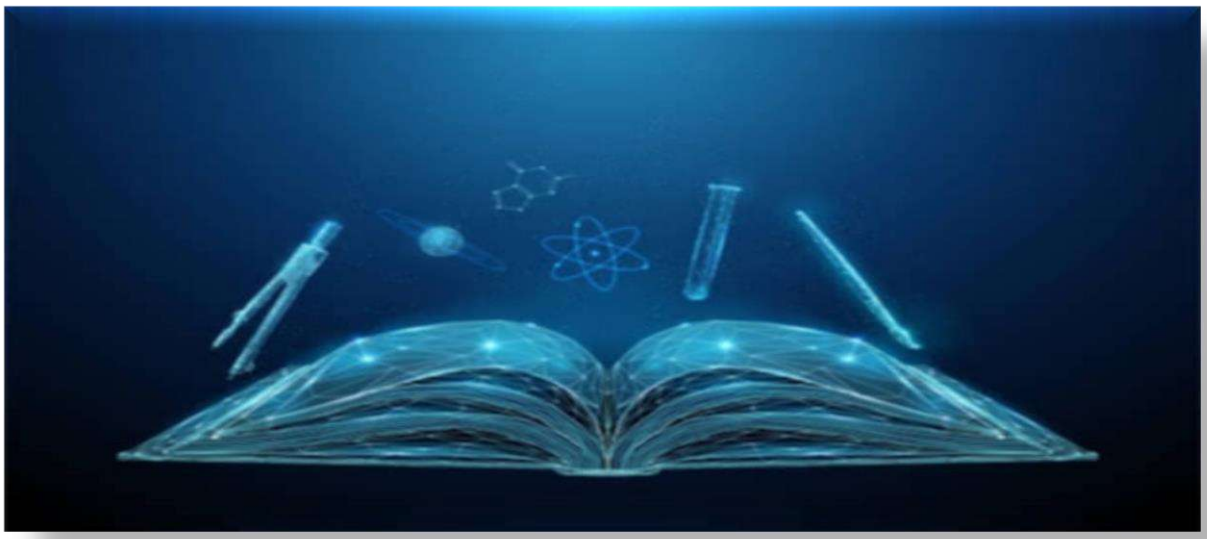


Figure II.9. Example of the determination of Urbach energy.

Chapter III

Results and discussion



III.1. Structural Studies

III.1.1. FTIR Analysis

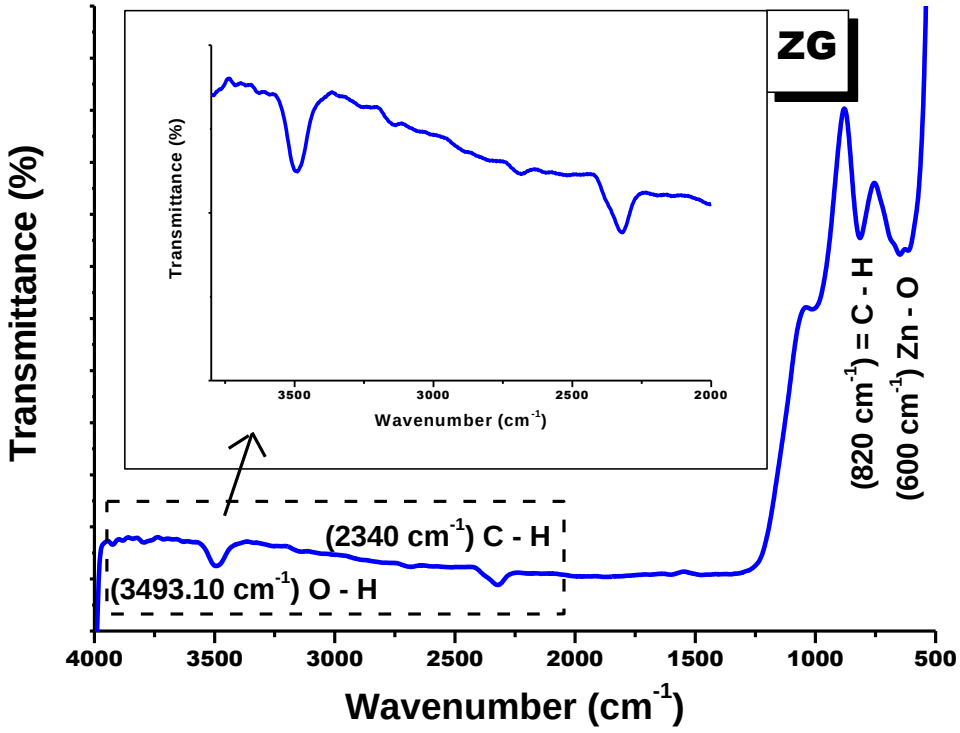


Figure III.1. FTIR spectrum of ZG thin film.

For the ZG thin film, the transmittance of Fourier Transform Infrared radiation in the 400–4000 cm^{-1} region is shown in Figure III.1. The stretching vibration of the Zn–O link is responsible for the observed absorption at 600 cm^{-1} [39]. The C–H bond, which is connected to alcohol and the other hydrocarbons in the solution, is responsible for the other transmittance minima, including the peak at 2340 cm^{-1}. O-H bonds are also responsible for the transmittance minimum at 3493.10 cm^{-1} [40], while the C-H mode vibration was detected at a peak of 820 cm^{-1} [41].

Table III.1. Comparative Analysis of vibrational modes of ZG thin film.

Possible bond	This study (cm^{-1})	Previous study (cm^{-1})	Reference
Zn–O	600	550	[39]
C–H O–H	2340 3493.10	2362 3451.8	[40]
C–H	820	881	[41]

Table III.1 provides a detailed comparison of the findings obtained in this study with those reported in previous research studies.

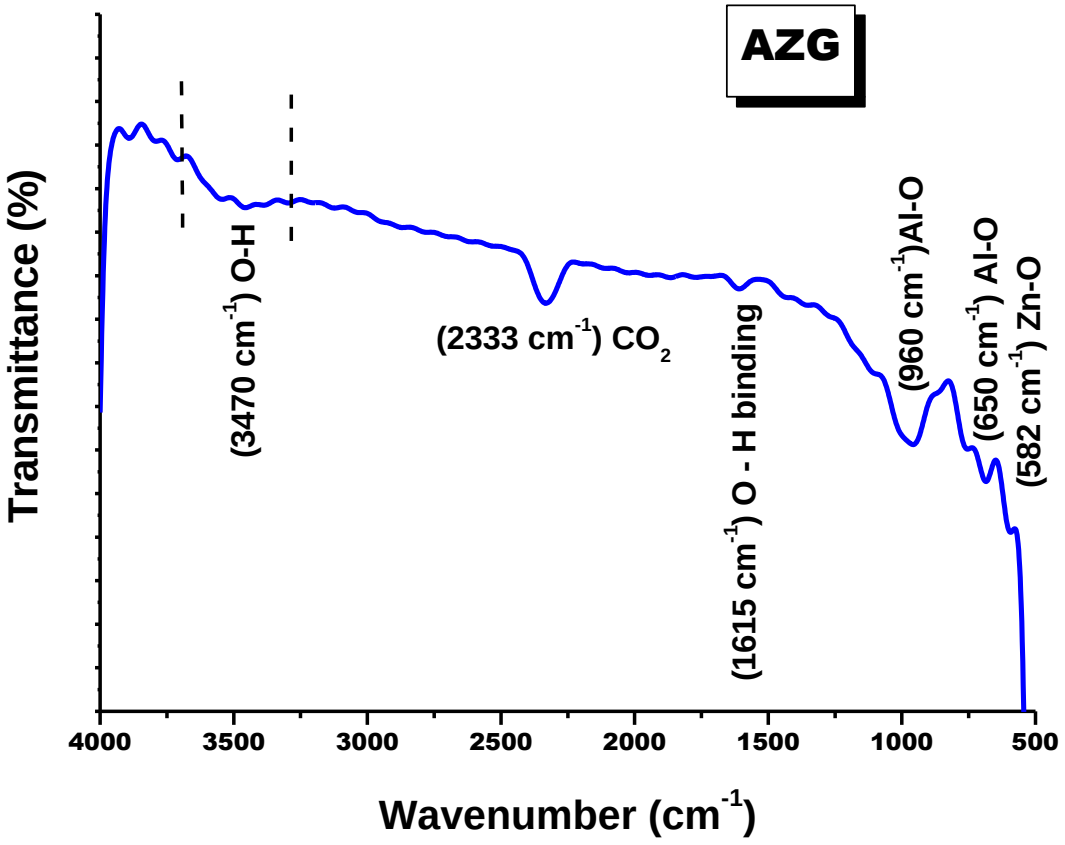


Figure III.2. FTIR spectrum of AZG thin film.

Figure III.2 presents the FT-IR spectrum of Z5A layer at middle infrared range. The peak observed at 3470 cm^{-1} is due to O–H stretching [42]. A peak has been observed about 2333 cm^{-1} respectively which arises from the absorption of atmospheric CO_2 on the metal cations. A sharp peak appeared about 650 cm^{-1} is a finger print of Al-O. The peak appeared about 582 cm^{-1} corresponds to the formation of Zn-O bond [39]. The band at 1615 cm^{-1} was assigned to the bending vibration of surface -OH .The weak band observed at 960 cm^{-1} correspond to the Al-O bond stretching vibration [43].

Table III.2. Comparative Analysis of vibrational modes of AZG thin film.

Possible bond	This study (cm^{-1})	Previous study (cm^{-1})	Reference
O–H	3470	3466	[42]
Al–O CO_2	650 2333	960 2350	[39]

Zn-O	582	550	
O–H Al–O	1615 960	1630 1075	[43]

Table III.2 provides a detailed comparison of the findings obtained in this study with those reported in previous research studies.

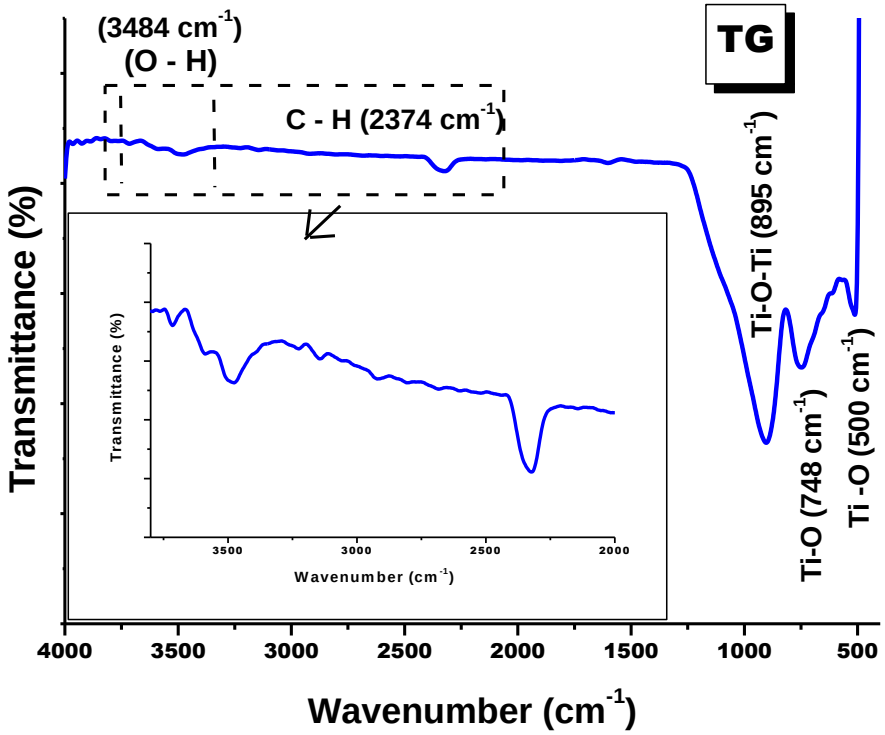


Figure III.3. FTIR spectrum of TG thin film.

Figure III.3 describes the Fourier transform infrared radiation in the range of 400–4000 cm^{-1} for the TiO_2 thin film. As it is observed the transmittance minima at 3484 cm^{-1} is attributed to O–H bonds Moreover the transmittance at 2347 cm^{-1} is attributed to C–H bond which is related to alcohol and the other hydrocarbons in the solution [40]. The stretching vibration of the Ti-O groups in the anatase phase was found at 748 cm^{-1} and the Ti-O-Ti bonds in the TiO_2 thin film stretching vibration mode are responsible for the absorption band 895 cm-¹ [44]. Ti-O bending mode is observed at 500 cm^{-1}[45]. Table III.3 provides a detailed comparison of the findings obtained in this study with those reported in previous research studies.

Table III.3. Comparative Analysis of vibrational modes of TG thin film.

Possible bond	This study (cm^{-1})	Previous study (cm^{-1})	Reference
O–H C–H	3484 2374	3451.8 2262	[40]
Ti-O-Ti Ti–O	895 748	874 741	[44]
Ti–O	1615	1630	[45]

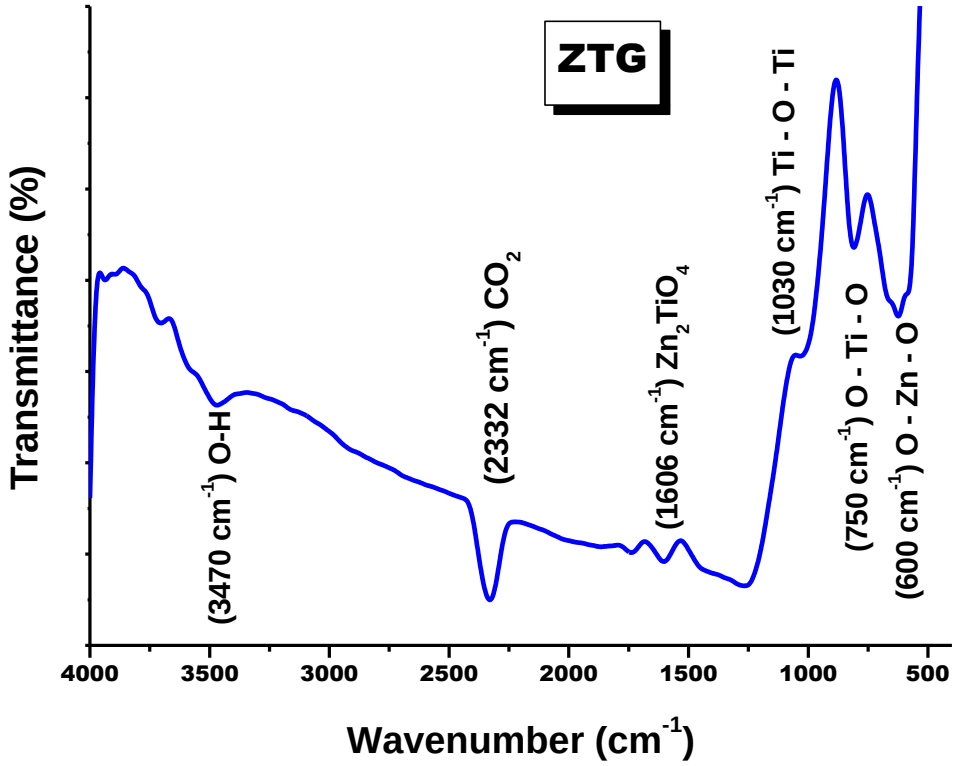


Figure III.4. FTIR spectrum of ZTG thin film.

Figure III.4 showed FTIR spectra of TZ thin films. The film spectrum is characterized by the presence of bands at 3470 cm^{-1} (OH stretching); Because TiO_2 is an oxide with O-Ti-O bonding in its chemical structure is represented by peak at 790 cm^{-1}. The vibration frequency of O-Zn-O bond groups is indicated by the peak at 600 cm^{-1} [46].The bands related to Ti-O-Ti skeleton bending vibrations could be observed at 1030 cm^{-1}, The band appearing at 2335 cm^{-1} is attributed to the adsorbed atmospheric CO_2 [47]. The vibration mode at the wavenumber of 1606 cm^{-1} can be attributed to the Zn_2TiO_4 bonds, which is consistent with the phase established in the XRD result [48].

Table III.4. Comparative Analysis of vibrational modes of ZTG thin film.

Possible bond	This study (cm^{-1})	Previous study (cm^{-1})	Reference
O–H O-Zn-O O-Ti-O	3470 600 790	3478 600 750	[46]
Ti-O-Ti CO_2	1030 2332	1053 2335	[47]

Table III.4 presents a comprehensive and systematic comparison between the results achieved in the current study and those documented in previous studies.

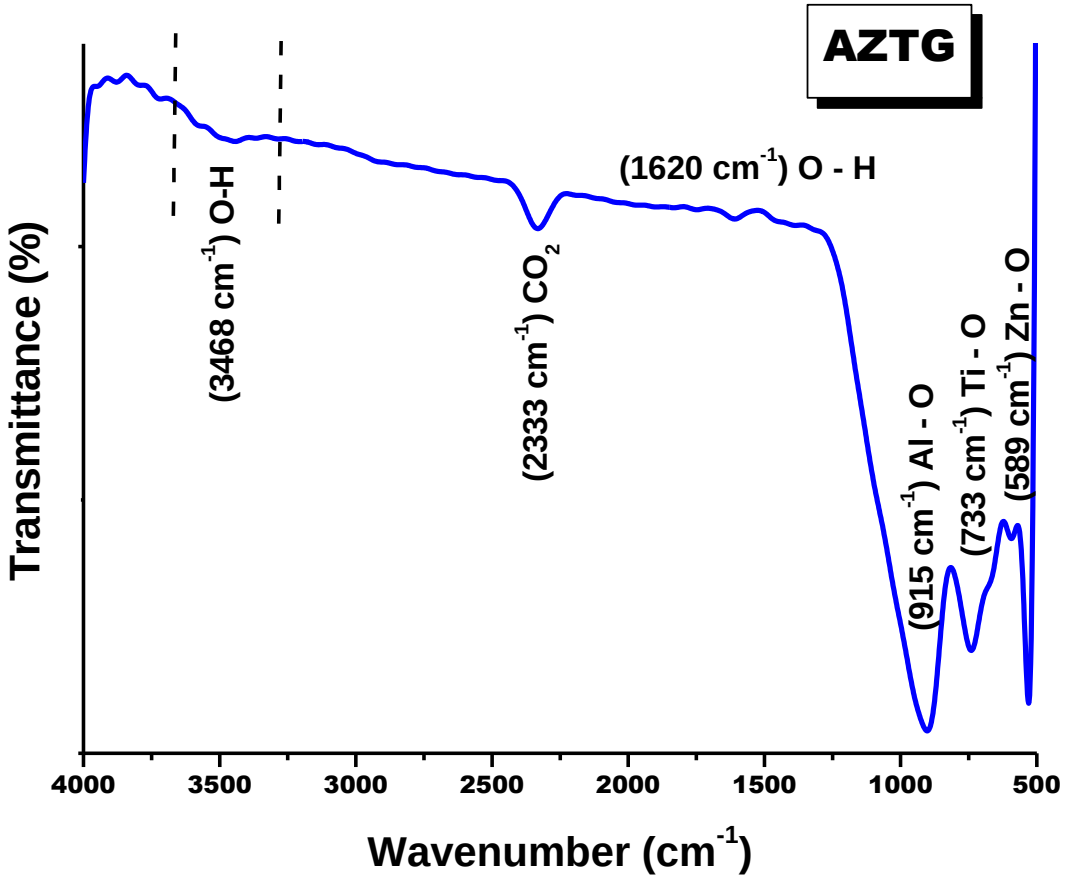


Figure III.5 FTIR spectrum of AZTG thin film.

Figure III.5 shows the FTIR spectra of TZ5A thin films. The absorption band around 589 cm^{-1} corresponds to the characteristic Zn–O stretching vibration [39]. The Ti–O stretching vibration is observed at 733cm^{-1}. The band at 2333cm^{-1} is attributed to the stretching vibrations of adsorbed atmospheric CO_2. The stretching vibrations of the –OH group are indicated by the band at 1620cm^{-1} [47]. The band at 915cm^{-1} is associated with the Al–O stretching vibration [49]. Finally, the peak at 3468 cm^{-1} corresponds to the stretching

vibration of the OH bond [46]. Table III.5 provides a comparison between the outcomes of earlier studies and the results obtained in our experiment.

Table III.5. Comparative Analysis of vibrational modes of AZTG thin film.

Possible bond	This study (cm^{-1})	Previous study (cm^{-1})	Reference
O–H	3470	3478	[46]
Al–O	915	960	[49]
Zn–O	589	550	[39]
Ti-O CO_2 O–H	733 2333 1620	713 2335 1628	[47]

III.2. Optical properties

III.2.1. UV–vis analysis

The experimental transmittance data for the synthesized ZnO thin films, namely ZG, AZG, ZTG, AZTG, and TG, across the wavelength range of 200 to 1100 nm, are illustrated in Figure III.6. All measurements are conducted at ambient temperature.

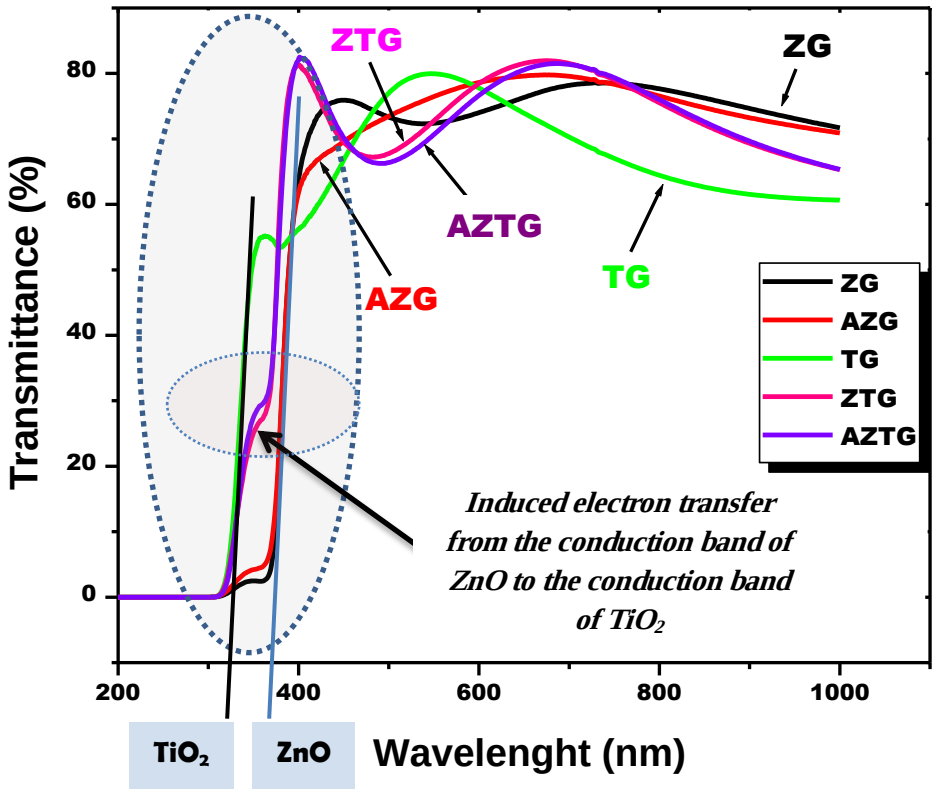


Figure III.6. Optical transmission spectra of ZG, AZG, TG, ZTG, and AZTG thin films.

Al-doped ZnO thin films serve as clear conductors in thin film solar cells [50], making it crucial to achieve films with great transparency in the visible spectrum.

The findings indicate that high transparency ranges from 68% to 82% in the visible spectrum (400–900 nm) for all samples, with the AZTG sample showing a peak transmittance of 82%. It demonstrates how well-suited the ZnO films made in these circumstances are for thin-film solar cell applications [51].Transmittance was found to increase proportionately with Al doping and to marginally decrease with the addition of the TiO_2 interlayer. The thickness of the films and the inherent optical characteristics of the TiO_2 interlayer are two of the reasons for this decrease in transmittance. Particularly when paired with ZnO films, the refractive index of TiO_2 can cause interference effects that alter the overall optical behavior, all thin films exhibit a significant absorption in the UV region (300–400 nm). Figure III.6 also shows the conduction band edge of ZnO is slightly higher than that of TiO_2 resulting in an induced electron transfer from the conduction band of ZnO to the conduction band of TiO_2 [63].

III.2.1.1. Calculation of the Refractive Index

The refractive index (n) of the developed samples can be estimated by utilizing the UV-visible spectra (Figure III.6). Using the relations II.3 and II.4 (Chapter II), the refractive index of these samples was calculated. Table III.6 provides a summary of the n values.

Table III.6. Presents the refractive indices for the ZG, AZG, TG ،ZTG and AZTG samples determined by UV-Visible transmission measurements.

Samples	Refractive index (n)
ZG	1.679
AZG	**1.839**
TG	2.050
ZTG	2.003
AZTG	**2.046**

The TiO_2 interlayer exerts a more pronounced influence on the refractive indexes than Al doping. The refractive index for the TiO_2-based sample (TG and AZTG) is higher (2.050 and 2.046 respectively) compared to ZG and AZG (1.679 and 1.839 respectively), which aligns with the higher optical density of TiO_2 [52].

III.2.1.2. Band gap and Urbach energy

a) Band gap

Tauc's approach (equation II.7) can be used to determine the optical band gap E_g of the spray-deposited ZnO thin films, such as ZG, AZG, ZTG, TG, and AZTG, from the transmission spectra.

Then, using a Tauc plot $(\alpha h\nu)^2$ vs. hν and projecting the linear portion of the curve to $((\alpha h\nu)^2=0$ (Figure III.7), the direct band gap of the resultant Al doped ZnO films was determined [41].

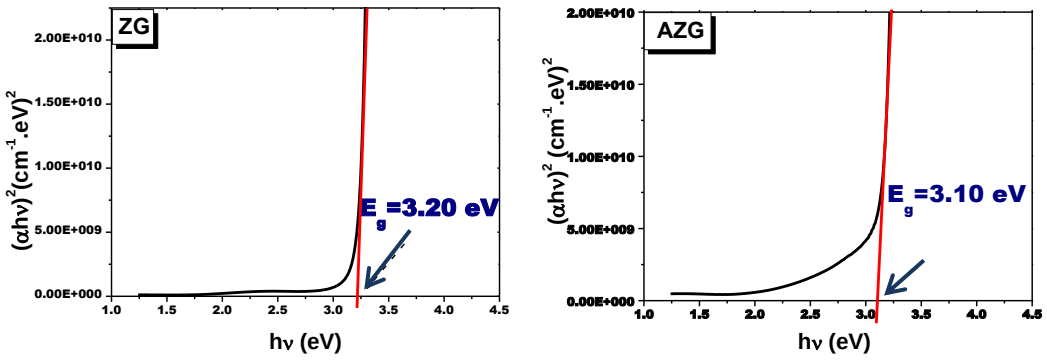


Figure III.7. Direct band gap energy (***Tauc's*** plot) determination of ZG and AZG.

At 0 and 5 wt % Al, respectively, the optical band gap values are calculated to be 3.20 and 3.10 eV. It indicates that when the amount of Al in AZG films increases, the band gap value drops. There will be more free electrons in the lattice as a result of the substitution of Zn^{+2} ions for Al^{+3} ions, increasing the likelihood of producing secondary levels in the energy gap around E_c. Along with a rise in the concentration of charge carriers in the n-type semiconductor, the deformation process also creates oxygen vacancies, which raise electrical conductivity. These ideal gap values are comparable to those found by ***A. Ashour et al*** [53, 54].

On the other hand, the indirect band gap of the resulting TiO_2 films was estimated by plotting $(\alpha h\nu)^{1/2}$ vs. hν, known as ***Tauc*** plot, and extrapolating the linear part of the plot to $(\alpha h\nu)^{1/2} = 0$ [52], (Figure III.8).

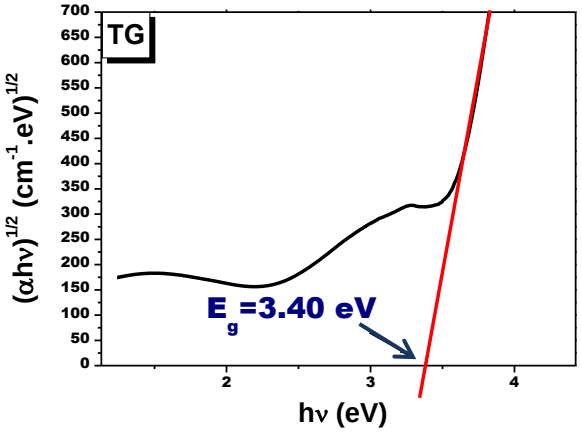


Figure III.8. Indirect band gap energy (***Tauc's*** plot) determination of TG**.**

The value of the indirect optical band gap (E_g) rose to 3.40 eV. The nanocrystalline form of the film may be the cause of the rise in the band gap value of TiO_2 film relative to bulk titanium oxide (E_g =3.20 eV), where the absorption edge will shift to a shorter wavelength of the radiation [55].

Finally, the band gap value (E_g) of the produced ZTG, and AZTG films, determined by the optical method, is obtained by extrapolating the linear portion of this graph to $(\alpha h\nu)^2 = 0$. The results are also presented in Table III.7.

The influence of the Al doping on gap energy appears to be more significant than the TiO_2 interlayer, as it enhances the gap energy.

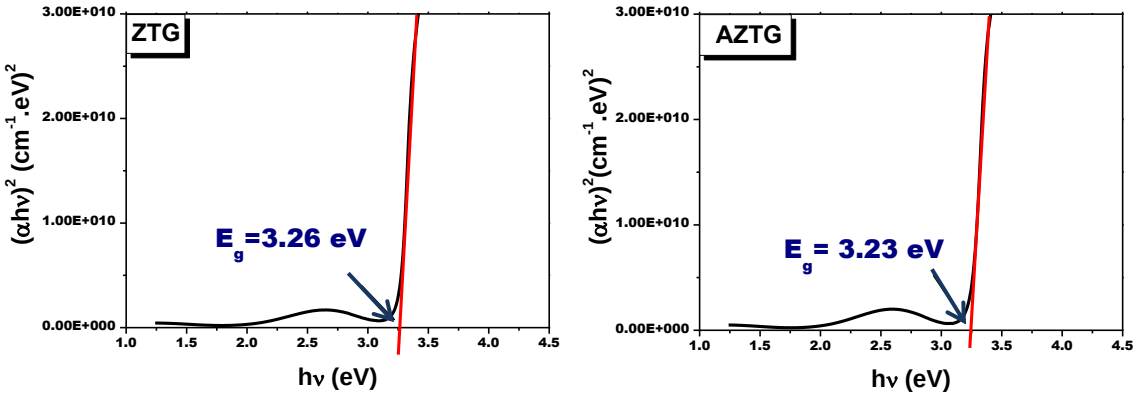


Figure III.9. Direct band gap energy (**Tauc's** plot) determination of ZTG and AZTG.

Table III.7. ***Tauc*** plot for the optical band gap estimation of ZG, AZG, TG, ZTG, and AZTG thin films.

Samples	Gap energy (eV)
ZG	3.20
AZG	3.10
TG	3.40
ZTG	3.26
AZTG	3.23

Numerous previous studies have investigated the energy band gap for ZnO and TiO_2. For instance, ***El-Hossary et al.*** [56] demonstrated that the energy band gap of ZnO varies between 3.14 and 3.35 eV, depending on changes in film thickness and surface morphology.

Similarly, ***El-Moula et al***. [57] reported that the E_g, for TiO_2 ranges from 3.12 to 3.49 eV. Other studies have shown that the band gap of ZnO is approximately 3.2-3.37 eV, depending on the crystal quality of the films. The results revealed that the TiO_2 interlayer increases the energy band gap from 3.20 eV to 3.26 eV. This change in the energy band gap may be attributed to the interaction between the two layers ZnO and TiO_2, promotes interfacial carrier transfers due to their matching band edge configurations. This Transfer increases the concentration of carriers in both the conduction and valence bands, which influences the electronic structure and subsequently alters the energy band-gap value [58, 59].

b) Urbach energy

Due to lattice instability in poorly crystalline materials, such as the ZnO structure, the density of electron states extends into the band gap [60]. The referenced tail is termed Urbach energy (meV), as indicated by equation II.8.

Plotting ln (α) vs. hν and the determined inverse slope of the ln (α) close to the band gap (Figure III.10) [61]. Can therefore be used to estimate the Urbach energy.

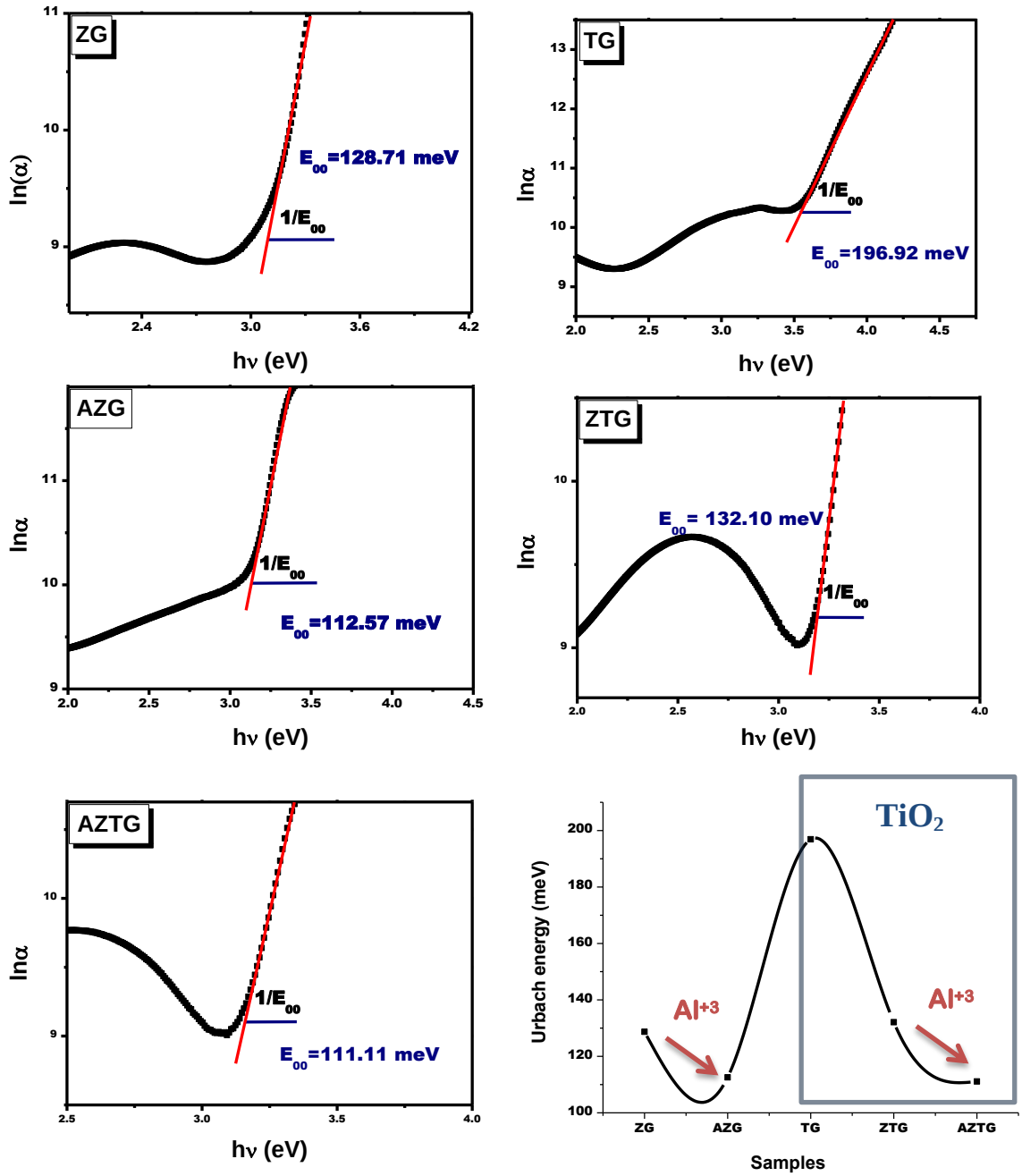


Figure III.10. Plots of Lnα as a function of photon energy for Urbach energy estimation of ZG, AZG, TG, ZTG, and AZTG thin films.

The results are shown in Table III.8. The band gap variation is consistent with a slight drop in the Urbach energy value as the Al content increases. Furthermore, the thin films that are created have more structural defects and disorders when TiO_2 is added as an interlayer for ZnO/glass.

Table III.8. Estimated Urbach energy of ZG, AZG, TG, ZTG, and AZTG thin films.

Samples	Urbach energy (meV)
ZG	128.71
AZG	112.57
TG	196.92
ZTG	132.10
AZTG	111.11

Figure III.10 and Table III.8 display the variations of the calculated band tail width E_{00} of the spray-deposited undoped and Al-doped ZnO films with and without a TiO_2 interlayer. With values increasing from 128.71 meV in the ZG sample to 132.10 meV in the ZTG sample, the disorder or Urbach energy increased with a TiO_2 interlayer. This suggests that the increased defect density brought about by the incorporation of a TiO_2 layer results in greater structural disorder (keeping in mind that the Urbach energy peaked in TG at 196.92 meV). In contrast, the Urbach energy dropped from 128.71 meV in ZG to 112.57 meV in AZG, presumably as a result of particular Al–O bonds that may lessen the material's electrical instability [62].

Conclusion

Conclusion

In this study, undoped and aluminum-doped ZnO thin films were fabricated using a spray pyrolysis and deposited onto glass substrates, with and without a TiO_2 interlayer. The synergistic effects of TiO_2 and Al doping on the structural and optical properties of ZnO were investigated. These features are characterized using Fourier transform infrared spectroscopy and a UV-visible spectrophotometer, in which we observe:

- **FTIR** analysis showed significant changes in the structural properties of ZnO due to the combined influence of TiO_2 and Al doping.
- The optical transmission spectra of fabricated films show an average high transmittance of ~ 65–82% in the visible region.
- The energy band gap increases from 3.10 to 3.40 eV. The highest band gap was shown in TiO_2 thin film, which was 3.4 eV while the band gap of ZnO was 3.23 eV. the Al doped ZnO films got the lowest energy band gap, which was 3.1eV.
- The results revealed that as the TiO_2 interlayer exerts a more pronounced influence on the refractive indexes of ZnO films than Al doping.
- The refractive index for the TiO_2-based sample (T and AZTG) is higher (2.050 and 2.046 respectively) compared to ZG and AZG (1.679 and 1.839 respectively), which aligns with the higher optical density of TiO_2.

Generally, the results provide accurate information about the physical and optical properties of the spray-deposited undoped and Al-doped ZnO films on a TiO_2 interlayer, demonstrating the adequacy of ZnO layers as a low optical absorption in the visible range in solar cell applications.

REFERENCES

REFERENCES

[1] F. T. Z. Toma, M. S. Rahman and K. H. Maria, "A review of recent advances in ZnO nanostructured thin films by various deposition techniques," Discover Materials, vol. 5, n°. 1, pp. 60, 2025.

[2] C. M. Firdaus, M. S. B. Shah Rizami, M. Rusop, and S. Rahmatul Hidayah, "Characterization of ZnO and ZnO: TiO_2 thin films prepared by sol-gel spray-spin coating technique," in Proc. Eng, vol. 41, pp. 1367–1373, 2012.

[3] MR. Qais M. Al-Bataineh, MR. Tariq O. Samara, MISS. Kholoud A. Al-izzy. "Optical properties of hydrophobic ZnO nano-structure based on antireflective coatings of $ZnO/TiO_2/SiO_2$ thin films". Physica B*:* Condensed Matter, vol. 593, pp. 412263, 2020.

[4] H. Dixit, B. P. Antwerpen, "First-principles electronic structure calculations of transparent conducting oxide materials". PhD, Universiteit Antwerpen.Belgium, 2012.

[5] Kh. Afzal, "Synthèse de Cuprates de Strontium ($SrCu_2O$) par MOCVD comme couche mince d'oxyde transparent conducteur de type P", Thèse Pour obtenir le grade de Docteur de L'unversite de grenoble, 2011.

[6] A. Yahia, Optimization of indium oxide thin films properties prepared by sol gel spin coating process for optoelectronic applications, Doctoral Thesis, University of Biskra, 2020.

[7] N. Abdelouahab, Preparation and characterization of thin films nanostructures based on ZnO and other oxides. Doctoral Thesis, University of Oum El Bouaghi, 2019.

[8] A. Saadi, rotational speed and solvent effect on the structural and optical properties of ZnO thin films prepared by sol-gel (spin coating) method, Final Dissertation in Master, University Med Khider of Biskra, 2013.

[9] Ch. Khelifi, "Tin dioxide SnO_2 thin films deposited by ultrasonic spray technique Properties and Applications", Doctorate thesis, Med Khider University-Biskra, 2018.

[10] R. Benmerad," Effect of Cr doping on optical and electrical properties of ZnO thin films deposited by spray pyrolysis technique". PhD Thesis. Université Echahid Chikh Larbi Tebessi-Tebessa, 2023.

[11] H. Serrar, A. Bouabellou, Élaboration et caractérisation de couches minces à base d'oxydes،these presentee pour obtenir le diplome de doctorat en sciences en physique، Université des frères Mentouri Constantine 1, 2019.

[12] F. Amraoui, I. Gharbi, "The Influence of Calcination Temperature on Properties of Thin films of Zinc-Oxide (ZnO) elaborated by Sol-gel (Dip-coating)", Master Memory, Mohamed Khider University of Biskra, 2022.

[13] M. Dahnoun, "Preparation and characterization of Titanium dioxide and Zinc oxide thin films via Sol-Gel (spin coating) technique for optoelectronic applications", Doctorate Thesis, University Mohamed Khider of Biskra, 2020.

[14] N. Ben Nouh, A. Saidi, "Développement de films minces d'oxydes transparents conducteurs", Mémoire de Master, Université Kasdi Merbah Ouargla, 2021.

[15] N. Chahmat, "Treatment of zinc oxide and study of its surface physicochemical properties", Doctorate's Thesis, Badji Mokhtar University-Annaba, 2014.

[16] F. Djenidi, "influence de taux de dopage par Sn et Al sur les propriétés des films d'oxyde de zinc (ZnO) élaborés par spray pneumatique pour des applications photocatalytiques", Mémoire De Master, Université Mohamed Khider de Biskra, 2024.

[17] F. Bedia, "caractérisations et optimisations des dépôts des couches minces d'oxyde de zinc (ZnO) en vue d'applications dans les énergies renouvelables", thèse de Doctorat, Université Abou Bakr Belkaïd – Tlemcen, 2015.

[18] Q. Sun, "Conducting ceramics based on ZnO co-doped by (Al, Ti, M_g): microstructure, electronic active defects and electrical properties". Thèse de doctorat. Le Mans Université; Institute of ceramics (Shanghai, Chine), 2020.

[19] S. Gasmi, "Elaboration des couches minces semi-conductrices pour des applications optoélectronique". Mémoire master académique. Université Kasdi Merbah Ouargla, 2021.

[20] T. Taouririt, "L'effet du débit de la solution sur les propriétés des couches minces d'oxyde de zinc (ZnO) déposées par spray pyrolyse", PhD Thesis, Université Med Khider Biskra, 2014.

[21] M. J. Gázquez, J. P. Bolivar, R. Garcia-Tenorio, F. Vaca, "A review of the production cycle of titanium dioxide pigment." Materials Sciences and Applications vol. 5, n°. 7, pp. 441-458, 2014.

[22] M. Landmann, E. Rauls and W. G. Schmidt, "The electronic structure and optical response of rutile, anatase and brookite TiO_2", J. Phys. Condens. Matter vol. 24, n°. 19, pp. 195503, 2012.

[23] S. D. Mo and W. Y. Ching, "Electronic and optical properties of three phases of titanium dioxide: Rutile, anatase, and brookite", Physical review B vol. 51, n°. 19, pp. 13023, 1995.

[24] Ch. Redjeb, M. Boudiar, "Elaboration et caractérisation des couches minces de TiO_2 dopé Zn obtenus par voie Sol-Gel" ، Memoire De Master، Université Larbi Tebessi - Tébessa، 2020.

[25] A. Sari, S. Bouchrit, "Elaboration et caractérisation des couches minces d'oxyde de cuivre non dopé", Master's Thesis, Larbi Tebessi University-Tebessa, 2017.

[26] S. Redjel, N. Mekhaznia, "Elaboration and characterization of tin oxide thin films deposited by spray pyrolysis", Master's thesis, Larbi Tebessi University-Tebessa, 2020.

[27] Dh. Rahal, T. Zerfaoui, "Elaboration of tin dioxide thin films by spray pyrolysis using different concentrations of solution and solvent", Thesis of Master, Larbi Tebessi University Of Tebessa, 2021/2022.

[28] J. Asim. M. Sh. Abdel-Wahab and H. Ahmed Hosny, "Advance deposition techniques for thin film and coating". IntechOpen vol. 2, n°. 3, pp. 138-147, 2017.

[29] K. Berima, R. Bouharra, "A study of properties of ZnO thin films deposited by spray pyrolysis technique on steel", Master Thesis, Mohamed Khider University of Biskra, 2020 / 2021.

[30] F. Khediri, "Etude expérimental des propriétés physiques des couches minces de ZnO ", Thèse de doctorat. Université Larbi Tebessi-Tébessa. 2022.

[31] A. Rouabah, O. Cheraitia, "Synthèse et caractérisation des couches minces de ZnO:Al élaborée par spray pyrolyse", Master Thesis, Dept. des Sciences de la Matière, Univ. Larbi Tebessi, Tébessa, Alegria, 2022.

[32] F. Mahcene, "Synthèse par Sol-gel et caractérisation structurale et optique de nano poudres de ZnO pures et dopées en Aluminium (0.1, 0.5, 0.75, 1.5 - 7, 10, 15 et 20 % at)", Doctorat en Sciences, Spécialité: Sciences des Matériaux, Université Mentouri Constantine 1, Algérie, 2021.

[33] A. Mujahid, F.L. Dickert, Molecularly imprinted sensors 1st Edition, pp. 125-159, June 2012.

[34] P.K. Manoj, B. Joseph, V.K. Vaidyan, D.S.D. Amma, "Preparation and characterization of indium-doped tin oxide thin films", Ceramics International vol. 33, n°. 2, pp. 273-278, 2007.

[35] J. Nidhal Nissan, "Effects of Cu-doping on optical properties of NiO, International Letters of Chemistry", Physics and Astronomy vol. 62, pp. 155-162, 2015.

[36] L. Herissi, "Development and characterization of thin layers of metal oxides intended for optoelectronic applications", Doctorate Thesis, Larbi Ben M'hidi University -Oum El Bouaghi, 2016.

[37] B. Maatoub. S. Fissah, "Study of the optical and electrical properties of tin oxide thin films deposited by spray pyrolysis", Master's Thesis, Larbi Tebessi University-Tebessa, 2022.

[38] D.B. M. Hoffman. S. Martin. W. Choi, "Environmental applications of semiconductor photo catalysis", Chemical Reviews, vol. 95, n°. 1, pp. 69-96, 1995.

[39] A. N. Mallika, A. Ramachandra Reddy, K. Sowri Babu, and K. Venugopal Reddy, "Synthesis and optical characterization of Aluminium doped ZnO nanoparticles," Ceramics International, Accepted Manuscript, vol. 40, n°. 8, pp. 12171-12177, 2014.

[40] F. Rahmani and M. Ardynanian, "Fabrication and characterization of ZnO/TiO_2 multilayers, deposited via spin coating method," Journal of Materials Science: Materials in Electronics, vol. 29, n°. 5, pp. 4285-4293, 2017.

[41] A. R. A. Rashid, H. K. Tazri, "Optical Properties of ZnO, TiO_2 and ZnO:TiO_2 Composite Films," Nano Hybrids and Composites, vol. 31, pp. 25–33, 2021.

[42] N. Ahammed, M. S. Hassan, and M. Hassan, "Effects of aluminum (Al) incorporation on structural, optical and thermal properties of ZnO nanoparticles," Materials Science-Poland, vol. 36, n°. 4, pp. 620–627, 2018.

[43] Y. Li, J. Wang, Y. Kong, J. Zhou, J. Wu, G. Wang, H. Bi, X. Wu, W. Qin, and Q. Li, "Micro/Nano hierarchical peony-like Al doped ZnO superhydrophobic film: The guiding effect of (100) preferred seed layer", Scientific Reports, vol. 6, n°. 1, pp. 19187, 2016.

[44] V. M. Mîndroiu, A. B. Stoian, R. Irodiă, R. Truscă, and E. Vasile, "Titanium Dioxide Thin Films Produced on FTO Substrate Using the Sol–Gel Process: The Effect of the Dispersant on Optical, Surface and Electrochemical Features", Materials, vol. 16, n°. 8, pp. 3147, 2023.

[45] L. Chougala, R. Kamble, et al, "A Simple Approach on Synthesis of TiO_2 Nanoparticles and its Application in Dye Sensitized Solar Cells," J. Nano- Electron. Phys., vol. 9, n°. 1, pp. 01025, Jan. 2017.

[46] H. Ali and N. Hameed, "Preparation of Cellulose Acetate Nanocomposite Films Based on TiO_2-ZnO Nanoparticles Modification as Food Packaging Applications," Journal of Applied Sciences and Nanotechnology, vol. 2, n°.3 , pp. 115 – 125, 2022.

[47] V. K. Landge, C.-M. Huang, V. S. Hakke, S. H. Sonawane, S. Manickam, and M.-C. Hsieh, "Solar-Energy-Driven Cu-ZnO/TiO_2 Nanocomposite Photocatalyst for the Rapid Degradation of Congo Red azo dye", Catalysts, vol. 13, n°. 2, pp. 1–15, 2023.

[48] T. Ivanova, A. Harizanova, T. Koutzarova, and B. Vertruyen, "Preparation and characterization of ZnO-TiO_2 films obtained by sol-gel method", Journal of Non-Crystalline Solids, vol. 357, n°. 11-13, pp. 2212–2216, 2011.

[49] F. Ajala, A. Hamrouni, A. Houas, H. Lachheb, B. Megna, L. Palmisano, and F. Parrino, "The influence of Al doping on the photocatalytic activity of nanostructured ZnO: the role of adsorbed water", Applied Surface Science, vol. 445, pp. 376-382, 2018.

[50] J. N. Ding, C. B. Tan, N. Y. Yuan, X. W. Feng, X. Y. Chang, and F. Ye, "The preparation and properties of Al-doped ZnO thin films as transparent electrodes for solar cell", Physics Procedia, vol. 32, pp. 789–794, 2012.

[51] A. Hafdallah, L. Herissi, N. E. Chergui, Z. Kebaili, M. S. Aida, and N. Attaf, "Structural and optical properties of ZnO thin films deposited by pyrolysis spray method: effect of Al doping", Nanotechnology Letters, vol. 2, n°. 1, pp. 11, Jul. 2018.

[52] X. Wang, G. Wu, B. Zhou, and J. Shen, "Optical constants of crystallized TiO_2 coatings prepared by sol-gel process", Materials, vol. 6, pp. 2819–2830, 2013.

[53] O. M. Abdulmunem, M. J. M. Ali, and E. S. Hassan, "Optical and structural characterization of aluminum doped zinc oxide thin films prepared by thermal evaporation system", Optical Materials, vol. 109, pp. 110374, 2020.

[54] A. Hafdallah, F. Ynineb, W. Daranfed, N. Attaf, and M. S. Aida, "Les propriétés structurales, optiques et électriques des couches minces de ZnO:Al élaborées par spray ultrasonique", Nature & Technologie, n°. 25, pp. 25–30, 2011.

[55] El-Hossary, F. M., Mohamed, S. H., Noureldein, E. A. El-Kassem, M. A. "Influence of rf power on growth, structural and optical properties of ZnO synthesized via vapor transport in inductively coupled plasma", Materials Science in Semiconductor Processing, vol. 120, pp. 105284, 2020.

[56] A.A.A. El-Moula, F.M. El-Hossary, M. Raaif, A. Thabet, M.A. El-Kassem," Effect of Cu metallic interlayer thickness on optoelectronic properties of TiO_2-based multilayers deposited by DC pulsed magnetron sputtering", Journal of Electronic Materials, vol. 50, pp. 2699-2709, 2021.

[57] P. Lv, W. Zheng, L. Lin, F. Peng, Z. Huang, F. Lai, "characteristics of ZnO/Cu2O thin film n–i–p heterojunction". Physica B: Condensed Matter, vol. 406, n°. (6-7), pp. 1253-1257, 2011.

[58] M. H. Fawey, A. A. Abd El-Mola, M. Abd El-Kassem, E. M. El Hossary, and T. Hashem, "Optical and structural properties of ZnO/TiO_2 bilayer thin films deposited by pulsed DC magnetron sputtering", J. Mater. Sci: Mater. Electron. vol. 36, pp. 3764, 2025.

[59] B.I. Stefonov, "Optically Transparent TiO_2 and ZnO Photocatalytic thin films via Salicylate-Based Sol Formulations", Coatings, vol. 13, n°. 9, pp. 1568, 2023.

[60] Ü. Özgür, Y. I. Alivov, Liu. C. Teke, A. Reshchikov, M. A. Doğan, A. H. Morkoç," A comprehensive review of ZnO materials and devices", Journal of applied physics, vol. 98, n°. 4, pp. 1-103, 2005.

[61] G. G. Riungu, S. W. Mugo, J. M. Ngaruiya, G. M. John, N. Mugambi, Optical band energy, urbach energy and associated band tails of nano crystalline TiO2 films at different annealing rates. American Journal of Nanosciences, vol. 7, n°. 1, pp. 28-34, 2021.

[62] Y. Geng, L. Guo, S.S. Xu, Q.Q. Sun, S.J. Ding, H.L. Lu, and D. W. Zhang, "Influence of Al Doping on the Properties of ZnO Thin Films Grown by Atomic Layer Deposition", Physical Chemistry C, vol. 115, n°. 24, pp. 12317–12321, Jun 2011.

[63] N. N. Khusna, H. Pujiarti, R. Kurniawan, "Structural and Optical Characteristics of Multilayer ZnO Nano rod: TiO_2 by DC Magnetron Sputtering for Dye Sensitized Solar Cell (DSSC) Application". In E3S Web of Conferences, Vol. 473, pp. 03005, 2024.